Hydrolysis of Metal Dioxides Differentiates d-block from f-block Elements: Pa(V) as a 6d Transition Metal; Pr(V) as a 4f "Lanthanyl"

Phuong D. Dau[1], Monica Vasiliu[2], Richard E. Wilson[3], David A. Dixon[2*], John K. Gibson[1*]

[1]Chemical Sciences Division. Lawrence Berkeley National Laboratory, Berkeley, CA 94720 USA

[2]Department of Chemistry, The University of Alabama, Tuscaloosa, AL 35401 USA

[3]Chemical Sciences and Engineering Division Argonne National Laboratory, Lemont, IL 60439 USA

*Corresponding author email: dadixon@ua.edu; jkgibson@lbl.gov

Abstract

Gas-phase reactions of pentavalent metal dioxide cations $M^{V}O_2^{+}$ with water were studied experimentally for M = V, Nb, Ta, Pr, Pa, U, Pu and Am. Addition of two H_2O can occur by adsorption to yield hydrate $(H_2O)_2M^{V}O_2^{+}$, or by hydrolysis to yield hydroxide $M^{V}(OH)_4^{+}$. Displacement of H_2O by acetone indicates hydrates for Pr^{V}, U^{V}, Pu^{V} and Am^{V}, whereas non-displacement indicates hydroxides for Nb^{V}, Ta^{V} and Pa^{V}. Computed potential energy profiles agree with the experimental results, and furthermore indicate that acetone unexpectedly induces de-hydrolysis and displaces two H_2O from $(H_2O)VO(OH)_2^{+}$ to yield $(acetone)_2VO_2^{+}$. Structures and energies for several M^{V}, as well as for Th^{IV} and U^{VI}, indicate that hydrolysis is governed by involvement of valence f versus d orbitals in bonding: linear f-element dioxides are more resistant to hydrolysis than bent d-element dioxides. Accordingly, for early actinides, hydrolysis of Th^{IV} is characteristic of a 6d-block transition metal; hydration of U^{V} and U^{VI} is characteristic of 5f actinyls; and Pa^{V} is intermediate between 6d and 5f. The praseodymium oxide cation $Pr^{V}O_2^{+}$ is assigned as an actinyl-like *lanthanyl* with properties governed by 4f bonding.

Introduction

Metal-oxo bonds are ubiquitous for metals, particularly so for very electropositive d-block and f-block elements. Common metal-oxygen bonds include M-OH_2 dative bonds to water in hydrates, M=O double (or higher order) bonds in oxides, and M-OH single bonds in hydroxides such as can result from hydrolysis. As relative stabilities of these metal-oxygen bonds underlie much chemistry, understanding them is essential. Despite the key role of hydrolysis in metal ion chemistry, it remains inadequately understood for species such as V^V,[1-5] Nb^V, and Ta^V.[6-8] For these group 5, d-block metals, the pentavalent solution species is not simple MO_2^+ but rather more complex and indeterminate oligomers $Nb_6O_{19}^{8-}$.[6] Hydrolysis of another group 5 metal, the early 5f actinide Pa, appears to reveal chemistry similar to d-block transition metals rather than prototypical 5f actinyls,[9, 10] though the underlying basis for this chemistry remains cloudy.[11]

Structures of simple metal dioxides illuminate the nature of their bonding. A classic example is the linear versus bent structures of isoelectronic UO_2^{2+} and ThO_2, a difference attributed to bonding—specifically back-bonding from O^{2-}—that involves 5f-orbitals of U, contrasting with 6d-orbital involvement for Th.[12] The issue of differing influences of f- versus d-orbitals on bonding in lanthanide and actinide compounds has been deliberated extensively.[13-21] Thorium(IV) can be considered as the first 6d transition metal element,[22] and uranium(IV) as the first true 5f actinide, reflecting decreasing energy of 5f relative to 6d orbitals with increasing nuclear charge.[23] The shift from d-block ThO_2 to f-block UO_2^{2+} suggests that isoelectronic PaO_2^+ could be intermediate in character,[11, 21] raising the issue of whether it is more like a d-block transition metal dioxide or a 5f actinyl.[24] For the 4f lanthanide analogue of Pa, praseodymium, the pentavalent oxidation state has been identified only in gas-phase compounds such as PrO_2^+ and NPrO.[25, 26] The chemistry of Pr^V has been assessed for the PrO_2^+ moiety embedded in a gas-phase nitrate anion complex.[27] Although bare PrO_2^+ has been reported, and elegantly characterized by infrared spectroscopy to reveal a linear structure,[25] its chemistry is unexplored such that it remains uncertain whether it exhibits chemical characteristics more similar to d-block dioxides or f-block actinyls. If actinyl-like, Pr^V would be *praseodymyl*, the first *lanthanyl*, to borrow a term from Ionova et al.[28] Although CeO_2^+ has been reported to have a linear structure, the high reactivity of the intermediate order Ce-O bonds indicate that it does not exhibit actinyl-like chemical character.[29] It should be noted that we adopt the conventional definition of actinyls, and thus also *lanthanyls*, as linear metal dioxo cations with short multiple bonds between the metal and oxygen. Goals of the current work included elucidation of the chemistry of pentavalent Pa and Pr, specifically whether they behave more like f-block or d-block elements.

An approach to explore metal-oxygen bonding is the relative propensity for formation of hydrates, hydroxides, and oxides, as assessed by thermodynamics and kinetics for interconversion between isomers containing these motifs.[30, 31] A dihydrated dioxide cation, $(H_2O)_2M^VO_2^+$, has two M=O oxo bonds and two M-OH_2 dative bonds to water, which could transform to four M-OH hydroxide bonds in isomeric $M^V(OH)_4^+$. Energies and barriers associated with hydrate-hydroxide isomer interconversion elucidate relative stabilities of the incorporated bonds. Such transformations are simplified for isolated complexes in the gas phase, absent solvation and other coordination effects.[32-34] A gas-phase study of partial hydrolysis of Pa^V found that addition of H_2O to PaO_2^+ yields both hydrate $(H_2O)PaO_2^+$ and hydroxide $PaO(OH)_2^+$, in qualitative accord with solution chemistry of Pa.[35]

We here examine the gas-phase reactivity of several metal dioxide cations with water. For the experiments, $M^{V}O_2^+$ ions were generated by electrospray ionization (ESI), where M = V, Nb, Ta, Pr, Pa, U, Pu and Am. An ion trap mass spectrometer was employed to study reactions of MO_2^+ with two H_2O, which can yield hydrate $(H_2O)_2MO_2^+$ or hydroxide $M(OH)_4^+$. As these isomers cannot be differentiated by their mass/charge ratios alone, which are identical for different isomers, the product structures were probed by reaction with acetone under the premise that H_2O in a hydrate will be replaced by such a stronger Lewis base, but H_2O in a hydroxide like $M(OH)_4^+$ will not. Results suggested hydrates for V^{V}, Pr^{V}, U^{V}, Pu^{V} and Am^{V}, but hydroxides for Nb^{V}, Ta^{V} and Pa^{V}, which portrays the 4f lanthanide Pr^{V} as acting like a 5f actinyl, and actinide Pa^{V} as d-block-like. Density functional theory (DFT, B3LYP) and coupled cluster CCSD(T) computations were performed for pertinent reactions of dioxides $M^{V}O_2^+$ for M = V, Nb, Ta, Pr, Pa, U, Pu, and Am, as well as for $Th^{IV}O_2$ and $U^{VI}O_2^{2+}$. Computation and experiment are in accord, except for the predictions that VO_2^+ partially hydrolyzes and NbO_2^+ fully hydrolyzes. The disparities for VO_2^+ and NbO_2^+ are reconciled in favor of the computational predictions that they are hydroxides by recognizing that addition of acetone to a hydroxide close in energy to a hydrate can induce conversion of the hydroxide to hydrate, followed by H_2O elimination. Such an acetone-induced dehydration process could naively, and incorrectly, be interpreted to indicate an initial hydrate structure. Hydrolysis for 6d-like $Th^{IV}O_2$ and hydration for 5f-like $U^{VI}O_2^{2+}$ are also predicted, further identifying Pa^{V} as intermediate between d-block and f-block elements. Resistance of Pr^{V} to hydrolysis supports the notion of *praseodymyl* as the first *lanthanyl* analog to the actinyls. Overall variations in energies and structures indicate that f-orbital bonding favors linear actinyl-like dioxides, whereas d-orbitals favor bent dioxides and tetrahedral hydroxides.

Experimental Methods

Caution! The Pa-231 U-238, Pu-242 and Am-243 isotopes employed in this work are radioactive. All experiments with these isotopes must employ special procedures in radiological laboratories.

The general approach has been described previously.[36, 37] Metal oxide cations MO_2^+ (M = V, Nb, Ta, Pr, Pa, U, Pu, Am) were produced by ESI of ~100 μM ethanol solutions (≤ 10% water) prepared by dilution of a stock solution of the metal. The aqueous stock solutions were as follows: 2.5 mM V_2O_5 and 25 mM HNO_3; ~10 mM (exact concentration not determined) K_2NbF_7 or K_2TaF_7 in excess HCl; 0.5 mM $PrBr_3$ and 50 mM HNO_3; 22 mM ^{231}Pa obtained by dissolving 1.7 mg $(NH_4)_2PaF_{7(cr)}$ in 1 M HF;[38, 39] 10 mM $^{238}UO_2(NO_3)_3^-$ (pH 1); 8 mM $^{242}PuO_2(ClO_4)_2$ (pH 1); 0.673 mM $^{243}AmO_2(NO_3)_2$ (pH 1). Radioactive isotope half-lives are 33,000 y for ^{231}Pa, $4x10^9$ y for ^{238}U, 373,000 y for ^{242}Pu, and 7370 y for ^{243}Am. Ions isolated in the ion trap of an Agilent 6340 quadrupole ion trap mass spectrometer undergo ion-molecule reactions at ~300 K.[40] Mass spectra were obtained in the positive ion mode using the following parameters: solution flow rate, 60 μL/h; nebulizer gas pressure, 12 psi; capillary voltage offset and current, ca. -3.5 kV and ~20 nA; end plate voltage offset and current, -500 V and ~200 nA ; dry gas flow rate, 4 l/min; dry gas temperature, 325 °C; capillary exit, 141.7 V; skimmer, 26.3 V; octopole 1 and 2 DC, 15.75 V and 3.13 V; octopole RF amplitude, 58.3 V_{pp}; lens 1 and 2, -4.8 V and -65.2 V; trap drive, 216.8. High-purity N_2 for nebulization and drying was the boil-off from liquid nitrogen. The background water pressure in the ion trap is estimated as ~10^{-6} Torr and was constant to within <10%.[41, 42] The He buffer gas pressure in the trap was constant at ~10^{-4}-10^{-3} Torr. Acetone (≥ 99.5%) was introduced into the trap through a variable leak valve to an indeterminate but constant (unless noted) pressure as confirmed by calibration using $UO_2(H_2O)^+$.[43]

Computational Methods

Geometries were optimized at the DFT level[44] with the hybrid B3LYP exchange correlation functional.[45, 46] The aug-cc-pVDZ basis sets[47, 48] were used for H and O; the cc-pVDZ-PP basis sets with effective core potentials were used for An = Th, Pa and U;[49-52] the Stuttgart small core relativistic effective core potential (60ECP) and basis set were used for Pu and Am;[53-55] the Stuttgart small core relativistic effective core potential (28ECP) with its accompanying segmented basis set were used for the lanthanide Pr;[56, 57] and aug-cc-pVDZ-PP were used for Group 5 transition metals V, Nb, and Ta.[58-60] Vibrational frequencies were calculated to show that the structures are minima. These calculations were performed using the Gaussian16 program system.[61]

The optimized geometries were then used in single point CCSD(T)[62-65] (coupled cluster theory with single and double excitations with a perturbative triples correction) calculations. The aug-cc-pV*n*Z basis sets were used for H and O; the cc-pV*n*Z-PP basis sets were used for Th, Pa and U; and aug-cc-pV*n*Z-PP were used for V, Nb, and Ta for n = D, T and Q. We note these basis sets as a*n*. The CCSD(T) energies were extrapolated to the CBS limit by fitting to a mixed Gaussian/exponential using the following equation:[66, 67] $E(n) = E_{CBS} + A \exp[-(n-1)] + B \exp[-(n-1)^2]$, where n = 2, 3, and 4 (DZ through QZ). Values obtained from this procedure are denoted as CBS.

All-electron single point CCSD(T) calculations using the 3rd-order Douglas-Kroll-Hess Hamiltonian[68-70] were performed at the DFT optimized geometries with the aug-cc-pV*n*Z-DK for H,[71] aug-cc-pwCV*n*Z-DK for O,[71, 72] cc-pwCV*n*Z-DK3 for Pu and Am,[73] and cc-pwCV*n*Z-DK3 for Pr[74] basis sets, for n = D, T for Pu and Am, and n = D, T, and Q extrapolated to the CBS limit for Pr, where possible. We note these basis sets as aw*n*-DK for Am and Pu and CBS-DK for Pr. The calculations included the correlation of the valence electrons and the 5s, 5p, 5d, 6s and 6p core-shell electrons for Pu and Am, the 4s, 4p, 4d, 5s and 5p core-shell electrons for Pr, and the 1s core-shell electrons of O. For Pu and Am, we used our previous reported results for the first addition of H_2O[30] and we performed calculations by changing the starting orbitals[75-77] for the CCSD(T) calculations from the Hartree-Fock orbitals to Kohn-Sham orbitals from DFT generated using the PW91 generalized gradient exchange-correlation functional.[78-80] as the PW91 orbitals resulted in much smaller values of the T_1 diagnostic.[81]

The open-shell calculations were done with the R/UCCSD(T) approach where a restricted open shell Hartree-Fock (ROHF) calculation was initially performed and the spin constraint was then relaxed in the coupled cluster calculation.[64, 82-84] The CCSD(T) calculations were performed with the MOLPRO 2018 program package.[85, 86]

The Natural Population Analysis (NPA) results based on the Natural Bond Orbitals (NBOs)[87] using NBO7[88, 89] are calculated using MOLPRO 2018 at the Hartree-Fock level. The calculations were done on our local UA Opteron- and Xeon-based Linux clusters as well as the Dense Memory Cluster at the Alabama Supercomputing Center. Selected calculations were done using Cascade in the Molecular Science Computing Facility (MSCF) in the Environmental Molecular Sciences Laboratory (EMSL) at Pacific Northwest National Laboratory (PNNL).

Results and Discussion

Experiments were performed for monopositive $M^{V}O_2^+$ containing a pentavalent metal. Computations were additionally performed for neutral $Th^{IV}O_2$ and dipositive $U^{VI}O_2^{2+}$. ***For simplicity, MO_2 without specified charge hereafter denotes all three types of species, $M^{V}O_2^+$, $Th^{IV}O_2$ or $U^{VI}O_2^{2+}$. The actual charge is indicated for formulations containing a specific metal.***

Differentiating Hydration from Hydrolysis

Gas-phase association of two H_2O with MO_2 can occur by net reactions (1a) - (1c).

(1a)	$MO_2 + 2H_2O \rightarrow (H_2O)_2MO_2$	*Hydration*
(1b)	$MO_2 + 2H_2O \rightarrow (H_2O)MO(OH)_2$	*Partial hydrolysis*
(1c)	$MO_2 + 2H_2O \rightarrow M(OH)_4$	*Full hydrolysis*

The experimental approach to differentiate products of reactions (1a) - (1c) was previously employed to distinguish hydrate $(H_2O)PaO_2^+$ from hydroxide $PaO(OH)_2^+$.[35] The premise is that a stronger Lewis base such as acetone (aco)[90] will displace "physisorbed" H_2O but not "chemisorbed" H_2O. The term "physisorbed" is used here for gas-phase complexes in which the H_2O ligand remains intact to yield a Lewis acid-base adduct, whereas "chemisorbed" is used for cleavage of a water ligand to yield a hydroxide. This specifically gas-phase terminology is not intended to suggest that condensed phase coordination complexes with strongly bound intact water ligands should similarly be referred to as "physisorption". Association to a metal center of intact ligands like H_2O and aco should not generally present large kinetic barriers, as the computational results described below illustrate, though with notable exceptions. Accordingly, displacement of such ligands should be governed primarily by energetics, specifically by stronger binding of aco versus physisorbed H_2O. In contrast to hydrates, elimination of chemisorbed H_2O from a hydroxide requires kinetically-hindering hydroxyl bond rearrangement. The resulting simple premise—revealed below as *too simple*—is that H_2O will be displaced from a hydrate, but not from two hydroxide groups with formation of H_2O and a metal oxo bond. Thus, products [a], [b] and [c] of reactions (1a), (1b) and (1c), respectively, are expected to exhibit the reactivity shown in Table 1. Included in Table 1 are predictions for aco adducts [a'], [b'] and [c'] that were, in some cases, studied in lieu of the simpler species. The results below demonstrate the utility of the H_2O-displacement approach, as well as a needed refinement to the premise underlying the approach.

The MO_2 ion of interest was produced by ESI of a solution containing dissolved M. The precursor solution metal species was not necessarily the pentavalent M^V found in the gas-phase species, which for the case of Pr^V is unknown in solution. Experiments in the ion trap proceeded as follows: (***A***) Isolation of MO_2 followed by its exposure to added aco and background gases; (***B***) Isolation of the product complex corresponding to addition of two waters, ***[MO_2 + 2H_2O]***, or two waters and one aco, ***[(aco)MO_2 + 2H_2O]***; and (***C***) Reaction of the isolated complex with aco and background gases, followed by final product identification. In step ***A***, competition between addition of aco and background H_2O determines what species is isolated in step ***B***. For M = V, Nb and Ta, sufficient ***[MO_2 + 2H_2O]*** was produced in step ***A***, but for M = Pr, Pa, U, Pu and Am, fast addition of aco required instead isolation of ***[(aco)MO_2 + 2H_2O]*** (Supporting Information Figure S1). Coordinating aco is presumed to insubstantially perturb the relative stabilities of hydrates and hydroxides, such that formation of [a'], [b'] and [c'] implies respective formation of [a], [b] and [c] (Table 1). Computational results indicate minor effects of spectator H_2O ligands on hydrolysis reactions, which suggests similarly minor effects of aco ligands (Supporting Information Figure S3).

In Table 1 three types of expected reactivity are identified: displacement of two H_2O by aco for [a] and [a']; displacement of one H_2O by aco for [b] and [b']; and no H_2O-displacement for [c] and [c']. Also indicated in Table 1 is the expected addition of aco to the primary products. Representative results for reactions of the complexes with aco (and background gases) are shown in Figures 1 and 2. For M = V^V, Pr^V, U^V, Pu^V and Am^V, displacement of two H_2O suggests reactants hydrate $(H_2O)_2MO_2$ (or $(aco)(H_2O)_2MO_2$). For M = Nb^V, displacement of one H_2O suggests $(H_2O)Nb^VO(OH)_2^+$. For M = Ta^V, no H_2O displacement suggests $Ta(OH)_4^+$. For M = Pa^V, separate reaction channels show displacement of one (minor) and two (major) H_2O, which suggests minor $(H_2O)PaO(OH)_2^+$ and mostly $Pa(OH)_4^+$. These assignments are summarized in Table 2 together with those from the computations. Reactions for long times (Supporting Information Figure 2) corroborate the results in Figures 1 and 2, and the assignments in Table 2. Refinement of the interpretations of the experiments, as discussed below, revises assignments of $(H_2O)_2VO_2^+$ to instead $(H_2O)VO(OH)_2^+$, and of $(H_2O)NbO(OH)_2^+$ to instead $Nb(OH)_4^+$, both revisions being in accord with the computational results. The experiments confirm previously reported dihydrates for actinyls UO_2^+ and PuO_2^+,[42] and extend this hydration behavior to americyl, AmO_2^+. Results for PrO_2^+ also indicate a dihydrate, $(H_2O)_2PrO_2^+$. It was previously established that the oxidation state in PrO_2^+ is Pr^V,[25] this being the only pentavalent lanthanide. The present results demonstrate that PrO_2^+ exhibits hydration chemistry that is also characteristic of actinyls so that *praseodymyl* is tentatively considered as the first *lanthanyl*, an assignment that is consistent with the reported structure,[25] and is further bolstered by computations discussed below.

For d-block transition metals, the results suggest H_2O adsorption by hydration to yield $(H_2O)_2VO_2^+$, partial hydrolysis to $(H_2O)NbO(OH)_2^+$, and full hydrolysis to $Ta(OH)_4^+$. Although these results are refined below, this initial trend invites comparison with the next two group 5 elements, Pr and Pa. Although both Pr^V and V^V evidently exhibit hydration, the computational results below indicate different underlying characteristics: PrO_2^+ is actinyl-like; VO_2^+ is not. Seeming contradictions between experiment and theory for V^V and Nb^V are reconciled by recognizing that addition of aco to their hydroxides can induce de-hydrolysis and H_2O elimination, as discussed in greater detail below. The experimental results for Pa^V indicate partial hydrolysis to $(H_2O)PaO(OH)_2^+$ as a minor channel, with mostly full hydrolysis to $Pa(OH)_4^+$, which is like Ta^V and quite unlike the actinyl(V) species U^V, Pu^V and Am^V.

Terminal Reaction Products

Results for long reaction times are summarized in Table 3 (see also Supporting Information Figure S2) where terminal products and corresponding maximum coordination numbers (CNs) are given. For the present conditions of low pressure and T≈300 K only complexes with inner-sphere metal-bound ligands are expected.[41, 42] Also, gas-phase CNs are often lower than in solution where the presence of additional far-field solvent molecules further stabilize inner-sphere ligands.[91] Thus, actinyls form pentahydrates in solution whereas tetrahydrates in gas phase.[42, 92] The M^V ionic radii (IR) for CN6 from Shannon are given in Table 3.[93] The IR for Pr^V in Table 3 is estimated by assuming a similar relationship for the following two groups: $Hf^{IV}/Ce^{IV}/Th^{IV}$ and $Ta^V/Pr^V/Pa^V$. For the first group: IR[Ce^{IV} = 0.87 Å] ≈ (0.3 x IR[Hf^{IV} = 0.71 Å] + 0.7 x IR[Th^{IV} = 0.94 Å]). This relationship applied to the second group yields: IR[Pr^V ≈ 0.74 Å] = (0.3 x IR[Ta^V = 0.64 Å] + 0.7 x IR[Pa^V = 0.78 Å]). It should be emphasized that this very crude estimate for IR[Pr^V] is not

whatsoever meant to be definitive, but rather only to provide guidance for approximate comparisons of bond distances below.

Terminal observed complexes were $(aco)_4MO_2$ with CN6 (M = U^V, Pu^V, Am^V), or $(aco)_3MO_2$ with CN5 (M = V^V, Pr^V). The lower CN of V^V is attributed to its smaller IR. As the estimated IR for Pr^V is comparable to the IR for Pu^V, the lower CN for Pr^V is not similarly rationalized. However, $(aco)_4PuO_2^+$ and $(aco)_4AmO_2^+$ were very minor products, such that the absence of detectable $(aco)_4PrO_2^+$ is not a significant disparity. Essentially similar behavior for PrO_2^+, PuO_2^+ and AmO_2^+ supports assignment of PrO_2^+ as an actinyl-like *lanthanyl*. CN6 complex $(aco)_4UO_2^+$ was abundant, presumably reflecting the relatively large IR for U^V. For Nb^V and Ta^V, CN6 complexes $(aco)_3NbO(OH)_2^+$ and $(aco)_2Ta(OH)_4^+$ were minor relative to those having one fewer aco. In contrast, CN6 $(aco)_3PaO(OH)_2^+$ and $(aco)_2Pa(OH)_4^+$ were prevalent; the higher CN for Pa^V presumably reflects its larger IR.

Association of background O_2 to $(aco)_3UO_2^+$ yielded $(aco)_3(O_2)UO_2^+$ (Figure 2b). Such O_2 addition for other complexes has been attributed to oxidation of U^V to U^{VI} in a superoxide.[42] Reaction for long times (Figure S2f) show that $(aco)_4UO_2^+$ is converted to $(aco)_3(O_2)UO_2^+$ by exothermic reaction (2). Like $(H_2O)_3(O_2)UO_2^+$,[42] $(aco)_3(O_2)UO_2^+$ is presumably a side-on bonded η^2-O_2 superoxide of U^{VI} with high CN7. The absence of an analog to reaction (2) for Np^V, Pu^V and Am^V reflects their higher M[VI/V] reduction potentials: 0.09 V for U^{VI}; 1.16 V for Np^{VI}; 0.94 V for Pu^{VI}; 1.60 V for Am^{VI}.[94]

(2) $(aco)_4UO_2^+ + O_2 \rightarrow (aco)_3(O_2)UO_2^+ + aco$

Results in Figure 2a indicate presence of both isomers $(aco)Pa(OH)_4^+$ and $(aco)(H_2O)PaO(OH)_2^+$. For longer reaction times (Figure S2e) the dominant product is $(aco)_2Pa(OH)_4^+$, with depletion of $(aco)_3PaO(OH)_2^+$ via exothermic reaction (3).

(3) $(aco)_3PaO(OH)_2^+ + H_2O \rightarrow (aco)_2Pa(OH)_4^+ + aco$

Potential Energy Profiles (PEPs)

Reactions (1a) - (1c) proceed by successive addition of two H_2O. Because the He pressure in the ion trap is at least 100 times greater than that of H_2O, products of the first H_2O addition experience many cooling collisions with He before encountering another H_2O molecule. Accordingly, association of two H_2O to MO_2 does not occur in a concerted manner but rather as separate sequential additions. These process are given by reactions (4a)-(4d) and (5a)-(5d) where, as above, MO_2 generically designates a metal dioxide with charge state neutral (ThO_2), monopositive (MO_2^+) or dipositive (UO_2^{2+}). Reaction with the first H_2O can occur by physisorption reaction (4a) or chemisorption reaction (5a). The product of (4a) can react with a second H_2O by three reaction pathways: physisorption (4b); chemisorption (4c); or chemisorption inducing conversion of the first H_2O to chemisorption (4d). The product of (5a) can react with a second H_2O by chemisorption (5b); physisorption (5c); or physisorption inducing conversion of the first H_2O to physisorption (5d).

(4a) $MO_2 + H_2O \rightarrow (H_2O)MO_2$ *1st physisorption*

(4b) $(H_2O)MO_2 + H_2O \rightarrow (H_2O)_2MO_2$ *2nd physisorption*
(4c) $(H_2O)MO_2 + H_2O \rightarrow (H_2O)MO(OH)_2$ *2nd chemisorption*
(4d) $(H_2O)MO_2 + H_2O \rightarrow M(OH)_4$ *2nd chemisorption/chemisorption*

(5a) $MO_2 + H_2O \rightarrow MO(OH)_2$ *1st chemisorption*
(5b) $MO(OH)_2 + H_2O \rightarrow M(OH)_4$ *2nd chemisorption*
(5c) $MO(OH)_2 + H_2O \rightarrow (H_2O)MO(OH)_2$ *2nd physisorption*
(5d) $MO(OH)_2 + H_2O \rightarrow (H_2O)_2MO_2$ *2nd physisorption/physisorption*

Computations were performed for each of these reaction pathways for M = Pa^V, U^V, Pu^V, Am^V, V^V, Nb^V, Ta^V, Pr^V, Th^{IV}, and U^{VI}. Energies for the pertinent species are in Table 4, and the resulting PEPs are shown in Figures 3-6, along with illustrative structures for the specific case of M = Pa^V. Coordinates for all structures are in Supporting Information. The MO_2, $MO(OH)_2$ and $M(OH)_4$ exhibit two essential structure types shown in Figure 7: *Pr-type* and *Ta-type*. Symmetries and bond angles are in Table S6.

Most energies used for the PEPs in Table 4 are CCSD(T)/CBS values, with exceptions identified there. Energies at the B3LYP level of theory are in SI Table S1. The largest differences between energies from B3LYP and CCSD(T) for a given M range from a low of 3.6 kcal/mol for Ta^V to a high of 19.4 kcal/mol for V^V. For most M, the largest differences are for $M(OH)_4$. The largest disparity between CCSD(T)/aT and CCSD(T)/CBS is only 2.9 kcal/mol, for the case of $(H_2O)_2TaO_2^+$.

Comparing Experiment and Theory

The reaction energetics of MO_2 with H_2O to yield $(H_2O)MO_2$ or $MO(OH)_2$ by reactions (4a) and (5a) are shown by the PEPs in Figure 3. For M = Pr^V, Pu^V and Am^V, TS1 prohibits hydrolysis to $MO(OH)_2$. A particularly revealing parameter is the isomerization energy to convert $(H_2O)MO_2$ to $MO(OH)_2$, plotted in Figure 8 (green data points). For M = U^{VI}, Pr^V, Pu^V, Am^V and U^V this isomerization is endothermic by at least 14 kcal/mol such that hydrate $(H_2O)MO_2$ is lowest in energy. For M = Nb^V, Ta^V and Th^{IV} this isomerization is exothermic by more than -17 kcal/mol so hydroxide $MO(OH)_2$ is lowest in energy. Although $VO(OH)_2^+$ is also predicted as the lowest energy structure, isomerization to it is exothermic by only -5.3 kcal/mol. For M = Pa^V, the isomerization is endothermic by only 0.6 kcal/mol so neither product is significantly preferred.[35] The energy to convert an actinide hydrate to hydroxide increases as the actinide 5f orbitals become stabilized from Pa^V to U^V to Pu^V to Am^V.

For the M^V that are predicted to first yield $MO(OH)_2$—V^V, Nb^V, Ta^V and perhaps Pa^V—a key question is whether association with a second H_2O results in hydrolysis reaction (5b) to yield $M(OH)_4$ or hydration reaction (5c) to yield $(H_2O)MO(OH)_2$, alternatives that are assessed by the PEPs in Figure 4. For none of the four does TS3 present a prohibitive barrier to hydrolysis. The ultimate product should thus be the lowest energy, which are summarized as the energies for isomerization of $(H_2O)MO(OH)_2$ to $M(OH)_4$ plotted in Figure 8 (blue data points). For M = Nb^V, Ta^V and Pa^V, this isomerization is exothermic by more than -12 kcal/mol so $M(OH)_4$ is the lowest energy structure. For M = V^V the isomerization is endothermic by 12.2 kcal/mol so

$(H_2O)VO(OH)_2^+$ is predicted to be more stable than $V(OH)_4^+$. The ultimate products are thus predicted to be $M(OH)_4$ for M = Nb^V, Ta^V and Pa^V, but $(H_2O)MO(OH)_2$ for M = V^V. Not shown in Figure 4, for simplicity, are TS2 barriers for addition of H_2O to $MO(OH)_2$ to yield hydrate $(H_2O)MO(OH)_2$. This transition state is associated with addition of water to hydroxides having the *Pr-type* structure with a quasi-linear O=M-OH moiety (Figure 7). TS2 thus exists for M = Pr^V, U^V, U^{VI}, Pu^V and Am^V. Notably, this barrier to simple hydration is remarkably substantial for the last two, at 8.2 and 19.1 kcal/mol, respectively, such that hydrates $MO(OH)_2$ for M = Pu^V and Am^V should not form under low-energy conditions. However, because these two species are among those that should not form $MO(OH)_2$ to start with, but instead form $(H_2O)MO_2$, these TS2 barriers do not impact the predicted courses of the reactions.

For the metals that are predicted to first yield $(H_2O)MO_2$—Pr^V, U^V, Pu^V, Am^V, and perhaps Pa^V—association with a second H_2O by reactions (4b), (4c) and (4d) is assessed by the PEPs in Figure 5. In all cases, addition of a second water as a solvating molecule is substantially exothermic. For M = Pr^V, Pu^V and Am^V the energies after $(H_2O)_2MO_2$ on the PEP are too high for further transformation. For these three M, TS4 is above the energy asymptote by at least 7.6 kcal/mol, TS3 is even higher, and formation of $M(OH)_4$ is endothermic by at least 9.6 kcal/mol. For M = U^V, $(H_2O)UO(OH)_2^+$ is kinetically accessible via TS4 but it is 9.1 kcal/mol higher in energy than $(H_2O)_2UO_2^+$. The PEP in Figure 5 for M = Pa^V shows that addition of H_2O to $(H_2O)PaO_2^+$ should yield $Pa(OH)_4^+$ as kinetically accessible and lowest energy, which is thus predicted as the final product for addition of H_2O to either $(H_2O)PaO_2^+$ or $PaO(OH)_2^+$.

The computational predictions are summarized in Table 2, where disparities between experiment and theory appear for M = V^V, Nb^V and Pa^V. For Pa^V the disparity is minor as the dominant and ultimate product in the experiments is the predicted species $Pa(OH)_4^+$. For M = V^V and Nb^V, the product inferred from experiment exhibits one less stage of hydrolysis than predicted. For Nb^V the disparity is between hydroxides $(H_2O)NbO(OH)_2^+$ and $Nb(OH)_4^+$, whereas for V^V it is between a hydrate and hydroxide. Hydrate $(H_2O)_2VO_2^+$ inferred from experiment is computed as actually 9.0 kcal/mol higher than $(H_2O)VO(OH)_2^+$. Inferred partial hydroxide $(H_2O)NbO(OH)_2^+$ is computed as 11.8 kcal/mol higher than $Nb(OH)_4^+$. This energy difference for V^V might reasonably be within error, but the implied error for Nb^V seems excessive. Rather than automatically assuming a large computational error, we surmise that displacement of H_2O by aco might occur for some hydroxides such as these, as elaborated in the following section. The demonstration below that such displacement can indeed occur indicates that the computations are likely valid whereas some inferences from experiment are likely not.

Another evaluation of the validity of the PEPs in Figure 3 is oxo-exchange reaction (6).

(6) $MO_2 + H_2{}^{18}O \rightarrow MO^{18}O + H_2O$

For reaction (6) to occur spontaneously, barrier TS1 to interconversion of $(H_2O)MO_2$ and $MO(OH)_2$ must lie below E = 0 (the energy of the separated reactants) on the PEPs in Figure 3.[43] In accord with the present PEPs, it was previously found that reaction (6) occurs for M = Pa^V and U^V, but not for Pu^V or Am^V.[30, 35] The PEPs further predict that Pr^V should not oxo-exchange, whereas U^{VI}, Th^{IV}, V^V, Nb^V and Ta^V should exchange. Schwarz and co-workers reported that reaction (6) does indeed occur for M = V^V.[95]

Can Acetone Displace H_2O from Hydroxides?

Although disparities between computations and experiments are modest, they motivate assessment of the assumption that acetone will displace H_2O from a hydrate but not from a hydroxide. PEPs in Figure 6 provide a basis to evaluate this hypothesis by considering reaction (7) where italicized *H_2O* and bold **OH** emphasize that the eliminated water, **H_2O**, derives from de-hydrolysis. The TS4 barrier on the PEP in Figure 6 determines whether the necessary $(H_2O)_2MO_2$ intermediate for occurrence of reaction (7) can form. This TS4 barrier is below the reactant asymptote ($E \leq 0$) for all eight M^V and for U^{VI}, lying above it only for Th^{IV}. Reaction (7) is exothermic for M = U^{VI}, U^V, Pu^V, Am^V, and Pr^V, nearly thermoneutral for M = Pa^V, endothermic by only 5.3 kcal/mol for M = V^V, and endothermic by at least 17 kcal/mol for Nb^V, Ta^V and Th^{IV}.

(7) $MO(\mathbf{OH})_2 + H_2O \rightarrow (H_2O)MO_2 + \mathbf{H_2O}$

The following specific assessment for V^V based on the PEP in Figure 6 indicates that reactions such as (8) and (9) cannot be excluded, this in conflict with the premise that acetone will not displace H_2O from a hydroxide. The energy for association of aco and VO_2^+ is computed as –75.9 kcal/mol at the CCSD/aT level (-79.8 at B3LYP), which is 20.8 kcal/mol more exothermic than for association of H_2O and VO_2^+. Accordingly, whereas reaction (7) is endothermic for M = V^V by 5.3 kcal/mol, reaction (8) is predicted to be exothermic by -15.5 kcal/mol. Furthermore, the PEP for reaction (8) and M = V^V, like that for V^V in Figure 6, is expected to lie fully below E = 0. This assessment illustrates that association of aco to a hydroxide might in some cases induce exothermic de-hydrolysis and H_2O elimination, with the direct implication that displacement of H_2O does not necessarily indicate a hydrate as was assumed for initial interpretation of the experimental results. As aco addition to V^V is 20.8 kcal/mol more exothermic than for H_2O, and $(H_2O)VO_2^+$ is only 5.3 kcal/mol higher energy than $VO(OH)_2^+$, reaction (8) is predicted to occur for M = V^V. Reaction (9) may similarly be viable for M = Nb^V as $(H_2O)NbO(OH)_2^+$ is a modest 11.8 kcal/mol higher in energy that $Nb(OH)_4^+$. However, when the hydroxide/hydrate energy difference is larger, such as for $(H_2O)TaO(OH)_2^+$ at 26.8 kcal/mol above $Ta(OH)_4^+$, aco should not induce H_2O-elimination from the hydroxide.

(8) $MO(OH)_2 + aco \rightarrow (aco)MO_2 + H_2O$
(9) $M(OH)_4 + aco \rightarrow (aco)MO(OH)_2 + H_2O$

Hydrate $(H_2O)_2VO_2^+$ was inferred from displacement of two H_2O to yield $(aco)_2VO_2^+$. Demonstrated viability of reaction (8) for M = V^V suggests that $(H_2O)VO(OH)_2^+$ might similarly react with aco to eliminate two H_2O and yield $(aco)_2VO_2^+$. Also, $Nb(OH)_4^+$ might react with aco as in reaction (9) to yield $(aco)NbO(OH)_2^+$. The general conclusion is that H_2O elimination from a hydroxide could be induced by aco addition, if the hydrate structure is only moderately—e.g. less than ~15 kcal/mol—higher in energy. This refinement of the premise underlying interpretation of the observations specifically resolves the apparent discord for V^V and Nb^V. Computed lowest-energy structures $(H_2O)VO(OH)_2^+$ and $Nb(OH)_4^+$ are now also considered sensible and valid from the perspective of the experimental results.

Isomerization Energies

Energies for isomerization reactions (10) - (12) plotted in Figure 8 reflect intrinsic relative stabilities of hydrates and hydroxides. These isomerization reactions provide insight into solution chemistry because, like a metal ion in solution, such conversion of a hydrate to hydroxide is not initiated and enabled by a bimolecular ion-molecule association as it is in distinctly gas-phase processes such as reactions (1a) - (1c). The ordering of metals on the abscissa in Figure 8 was identified as reflecting key structural trends discussed below. This ordering results in similar energies for isomerization reaction (10), to within less than 8 kcal/mol, for the first three M^V species, Pr^V, Pu^V and Am^V, followed by a regular decrease for the next five M^V. Placed at the far ends of the axis in this plot are U^{VI} and Th^{IV}, with the isomerization energy for U^{VI} intermediate between those for Pr^V and Pu^V, and that for Th^{IV} the lowest of all the M. The isomerization energies for Pa^V, U^V, Pu^V and Am^V are consistent those obtained in our prior work.[96] The previously reported isomerization energy for M = Np^V , 20.8 kcal/mol,[96] is between those obtained here for U^V (13.5 kcal/mol) and Pu^V (28.0 kcal/mol).

(10) $(H_2O)MO_2 \rightarrow MO(OH)_2$
(11) $(H_2O)MO(OH)_2 \rightarrow M(OH)_4$
(12) $(H_2O)_2MO_2 \rightarrow M(OH)_4$

The reaction (10) isomerization energies for f-elements Pr^V, U^V, Np^V, Pu^V and Am^V are positive such that $(H_2O)MO_2$ is more stable than $MO(OH)_2$ (Figure 8). For group 5 d-block elements V^V, Nb^V and Ta^V, these isomerization energies are negative such that $MO(OH)_2$ are more stable. The isomerization energy for Pa^V (0.6 kcal/mol) is so close to zero that Pa^V is intermediate in character between the f- and d-block species. The extremely favorable energy for $(H_2O)ThO_2$ to isomerize to $ThO(OH)_2$ indicates d-block character for the nominal 5f actinide Th^{IV}. The monotonic increase in isomerization energies across the actinide series from Pa^V to Am^V indicates lower relative stability of the hydroxide as 5f orbitals decrease in energy relative to 6d/7s.[23, 96] Another trend is decreasing isomerization energy from 3d-element V^V to 4d Nb^V to 5d Ta^V, and a further decrease to 6d Th^{IV}. The reaction (10) isomerization energy for Pa^V is lower than for actinyls, but not as low as for the distinct d-block elements, indicating its intermediate character.

As for reaction (10), the isomerization energies for reaction (11) plotted in Figure 8 show a trend for the d-block species of a decrease from endothermic for V^V to exothermic for Nb^V and Ta^V. The reaction is endothermic for Pr^V, U^V, Pu^V, and Am^V with the order being $Pr^V > Pu^V > Am^V > U^V$. In contrast to the energies for reaction (10), those for reaction (11) *increase* from Pa^V to V^V. The energy for Pa^V is significantly below that for V^V and slightly below that for Nb^V, with Pa^V thus lying between Nb^V and Ta^V. An alternative to energies for isomerization reactions (10) and (11), are those for combined isomerization reaction (12), which plotted in Figure 8 show Pa^V intermediate between V^V and Nb^V. Overall, the results in Figure 8 demonstrate that isomerization of Pa^V hydrates to hydroxides is more similar to d-block rather than f-block elements.

Notably, Pr^V is predicted to exhibit particularly unfavorable isomerization to hydroxides, with a high stability of hydrated $(H_2O)_2[O=Pr=O]^+$ *relative* to $Pr(OH)_4^+$. It should be emphasized that this does not suggest that PrO_2^+, or any Pr^V species, should be stable in condensed phase.

Stabilities of M^V towards reduction to M^{IV} can be roughly evaluated from fifth ionization energies, IE[M^{4+}],[97] which for the actinides increase from Pa (~44.3 eV) to Am (~50.0 eV)[98] in correspondence with increasing M[V/IV] reduction potentials.[94] Although the Pr[V/IV] reduction potential is not determined, IE[Pr^{4+}] = 57.53 ± 0.05 eV[98] is so high that reduction of Pr^V to Pr^{IV} should be very favorable, likely unavoidable in liquid water. The present results thus do not predict that Pr^V can be prepared in condensed phase but rather that *hypothetical* $Pr^VO_2^+$, like uranyl and other actinyls, would be resistant to solution hydrolysis to yield a Pr^V hydroxide. Instead of forming *praseodymyl* in solution, reaction of Pr^V with liquid water might result in hydrolytic reduction to species like $Pr^{IV}(OH)_n^{(4-n)}$ or $Pr^{III}(OH)_{n'}^{(3-n')}$ (n = 0-5; n´ = 0-4).

It might naively be expected that stronger M=O bonds should be more resistant to activation such as occurs in conversion of oxides to hydroxides. However, experimental bond dissociation energies for MO_2 (neutral or cation) to yield M (neutral or cation) and two O (neutral), plotted in Figure 8,[99, 100] show that lower metal oxide bond energies do not imply more favorable transformation to hydroxides. Oxides PaO_2^+, NbO_2^+, TaO_2^+ and ThO_2 have very strong M=O bonds, yet they are particularly susceptible to conversion of their hydrates to hydroxides. For example, the energy to dissociate TaO_2^+ (340 kcal/mol) is more than twice that for VO_2^+ (161 kcal/mol). Nonetheless, transformation of $(H_2O)_2MO_2$ to $M(OH)_4$ is substantially exothermic for M = Ta^V (ΔE = -61 kcal/mol), but slightly endothermic for M = V^V (ΔE = 3.2 kcal/mol). Energy barriers for transformation of $(H_2O)_2MO_2$ to $M(OH)_4$ are also lower for M = Ta versus V (Figure 5). As this apparent enigma illustrates, the energy to transform a hydrate to a hydroxide does not depend only on the strengths of the M=O (and M-OH_2) bonds that are disrupted, but also on the M-OH bonds that are created. Such an evaluation considering only M-O bonds assumes negligible differences between the O-H bonds disrupted in hydrates and created in hydroxides. A less stringent but adequate assumption is that changes in O-H bonds between hydrates and hydroxides may be significant but are similar for different metals. Overall energetics and kinetic barriers suggest that strong M=O bonds in MO_2 are associated with strong M-OH bonds in $M(OH)_4$. Relatively small differences in net energies of the four M-O bonds in $(H_2O)_2MO_2$ versus those in $M(OH)_4$ dictate the isomerization energetics. Although the Ta=O bonds in $(H_2O)_2TaO_2^+$ are very strong, the also very strong Ta-OH bonds in $Ta(OH)_4^+$ favor the latter isomer. As elaborated below, stabilities of dioxides versus hydroxides evidently reflect variations in efficacy of M=O versus M-OH bonding for different types of metal-based bonding orbitals.

Linking Energies, Structures, and Bonding

Relative stabilities of oxides and hydroxides reflect differences in bonding that are also manifested in structures, such as those summarized in Figure 7 and Table S6. A characteristic feature of the species in Figure 7 is a propensity for either a linear, or moderately bent "quasi-linear", or a highly bent O-M-O moiety in MO_2, $MO(OH)_2$ and $M(OH)_4$. The angles plotted in Figure 9 capture these tendencies. The MO_2 are linear "actinyl-like" for M = U^{VI}, Pr^V, Pu^V, Am^V, U^V and Pa^V, but highly bent for M = V^V, Nb^V, Ta^V and Th^{IV}. These two MO_2 structure types, linear *Pr-type* versus bent *Ta-type*, are characteristic respectively of valence f and d orbital involvement in bonding.[12, 101-104] A simple but durable concept to explain such structural differences is that dominance of back-bonding from O^{2-} 2p orbitals to the metal center is more effective for linear structures if the bonding is to f orbitals, and more effective for bent structures if it is to d orbitals.[12]

The underlying basis for the reality of these different structural motifs, linear and bent, has been convincingly rationalized by considering bonding in d-block transition metal oxides,[13, 104] and 5f actinyls.[103] It should additionally be remarked that such structure-bonding correlations are useful phenomenological approaches even absent full causal understanding, which is likely ultimately unattainable.

The angles in Figure 9 for $MO(OH)_2$ show that one of the two O=M-O_{OH} angles is highly obtuse (≥ 159°, "quasi-linear") for M = U^{VI}, Pr^V, Pu^V, Am^V and U^V, which also exhibit linear MO_2. The corresponding angle in $MO(OH)_2$ for M = V^V, Nb^V, Ta^V and Th^{IV} is highly bent like in MO_2. For M = Pa^V there is a distinct shift from linear actinyl-like PaO_2^+ to two highly bent O=Pa-O_{OH} angles in $PaO(OH)_2^+$. Referring to Figure 8, conversion of $(H_2O)MO_2$ to $MO(OH)_2$ is energetically favorable for d-block M = V^V, Nb^V, Ta^V and Th^V, where reactant and product have similar bent O-M-O angles. This conversion is energetically unfavorable for f-block M = U^{VI}, Pr^V, Pu^V, Am^V and U^V (as well as for Np^V [96]) that exhibit linear MO_2 and maintain quasi-linearity in $MO(OH)_2$. Nearly thermoneutral transformation of $(H_2O)PaO_2^+$, with a linear O=Pa=O unit, to bent $PaO(OH)_2^+$ suggests competition between f- and d-orbital participation, with Pa intermediate between 5f and 6d elements. As seen in Figure 8, the energy for isomerization of $(H_2O)PaO(OH)_2^+$ to tetrahedral $Pa(OH)_4^+$, a structure indicative of dominant 6d bonding,[13] is even more exothermic than the corresponding energy for $(H_2O)NbO(OH)_2^+$, which indicates d-block character for Pa^V.

The shift from linear/quasi-linear to bent structures is seen in Figure 9 to occur between Pa^V and V^V for MO_2; between U^V and Pa^V for $MO(OH)_2$; and between Pu^V and Am^V for $M(OH)_4$. Except for M = U^{VI}, Pr^V and Pu^V, the O_{OH}-M-O_{OH} angles in $M(OH)_4$ are within 3.1° of the ideal tetrahedral value of 109.5°. For M = U^{VI}, Pr^V and Pu^V there is substantial deviation from tetrahedral, with a "quasi-linear" O_{OH}-M-O_{OH} angle of greater than 150°. The result in Figure 8 that formation of $M(OH)_4$ from $(H_2O)_2MO_2$ is particularly energetically unfavorable for M = U^{VI}, Pr^V and Pu^V can be attributed to dominant f orbital bonding that favors linear structures such as found in the actinyl moiety. Results for U^V suggest a switch from f-orbital bonding in linear UO_2^+ to d-orbital bonding in tetrahedral $U(OH)_4^+$, where the T_d structure of the latter alternatively would be consistent with predominantly non-directional ionic bonding.

The satisfaction of listing the actinides in order of appearance across the series is disrupted on the abscissa in Figure 9. The basis for the ordering there as U^V-Am^V-Pu^V, rather than seemingly more natural actinide series progression of U^V-Pu^V-Am^V, is the variation in the structures of the $M(OH)_4^+$. The $MO(OH)_2^+$ for M = U^V, Pu^V and Am^V exhibit structures with a quasi-linear O=M-OH configuration that is characteristic of 5f orbital participation in covalent bonds. However, whereas $M(OH)_4^+$ for M = U^V and Am^V exhibit tetrahedral structures that evidently lack the structural constraint imposed by the 5f orbitals, the structure of $Pu(OH)_4^+$ retains a quasi-linear HO-Pu-OH configuration indicative of 5f bonding. This assessment seems to suggest that the participation of the 5f orbitals in the M-O bonds of $M(OH)_4^+$ may be greater for M = Pu^V versus M = U^V or Am^V. Although this potential interpretation is based on limited information, and is thus only tentative, similar maxima in actinide-oxygen bond covalency at or around Pu have been proposed for other oxo species, including actinyls.[105] Notably, the structure of $Pr(OH)_4^+$ features a quasi-linear HO-Pr-OH connectivity that is indicative of 4f orbital bonding.

Overall, the results indicate that formation of hydroxides from oxides is least favorable when linear structures are more strongly imposed by f orbital bonding. Essential characteristics of

Pr^{V}—linear PrO_2^+ resistant to hydrolysis to quasi-linear $Pr(OH)_4^+$—indicates substantial involvement of 4f orbitals in metal-oxygen bonding. The PrO_2^+ species exhibits a similar propensity towards linearity as uranyl(VI),[25] which for the latter is attributed to involvement of U 5f orbitals.[12] We infer substantial 4f bonding character for Pr^{V}, and assign PrO_2^+ as a *lanthanyl*, specifically *praseodymyl*.

The importance of lanthanide 4f and actinide 5f orbitals in bonding is related to their energies relative to other valence orbitals. Homologous pairs early in the two series exhibit the following ground-state atomic configurations (outside of the closed-shell Xe or Rn cores):[98]

La[$5d^1 6s^2$] / Ac[$6d^1 7s^2$]
Ce[$4f^1 5d^1 6s^2$] / Th[$6d^2 7s^2$]
Pr[$4f^3 6s^2$] / Pa[$5f^2 6d^1 7s^2$]
Nd[$4f^4 6s^2$] / U[$5f^3 6d^1 7s^2$]
Pm[$4f^5 6s^2$] / Np[$5f^4 6d^1 7s^2$]
Sm[$4f^6 6s^2$] / Pu[$5f^6 7s^2$]
Eu[$4f^7 6s^2$] / Am[$5f^7 7s^2$]

These atomic configurations illustrate that the energy of 4f orbitals relative to 5d orbitals is lower than for 5f relative to 6d.[23] A result of this difference is that lanthanides have 5d occupancy only for the first two members, La and Ce, whereas actinide 6d occupancy persists for the first five members, from Ac to Np, with the 5f fully below 6d only for Pu and beyond. Like Hf, Th has a d^2s^2 valence configuration and thus generally behaves like a d-block transition metal. Beyond Th, the 5f orbitals become partially occupied with a transition to 5f-like chemistry beginning at Pa. Although this assessment employs electronic configurations of atoms, it should also provide insight into trends for relative orbital stabilities, and occupancy, for these atoms in similar chemical environments. Thus, the nearly linear protactinyl moiety in $(H_2O)_2PaO_2^+$ is considered a manifestation of 5f orbital involvement, whereas its isomerization to tetrahedral $Pa(OH)_4^+$ suggests 6d involvement, a combination of bonding contributions that is consistent with the relative orbital energies for atomic Pa. Similarly, as atomic Pr, the lanthanide homolog of Pa, has valence 4f orbitals lower energy than 5d, the result is a nearly linear PrO_2^+ in $(H_2O)_2PrO_2^+$ that resists conversion to $Pr(OH)_4^+$.

Dative Bonding in Hydrates

Like the bare MO_2, the dihydrates $(H_2O)_2MO_2$ exhibit two basic structure types: *Pr-type* with nearly linear O=M=O, and *Ta-type* in which this moiety is highly bent. These structures are shown in Figure 10 together with selected bond angles. The specific structure of $(H_2O)_2ThO_2$ shown in Figure 10 is formally *Ta-type*, but it is distinctive in being pyramidal-like. The O=M=O angles in all $(H_2O)_2MO_2$ are within a few degrees of those in bare MO_2, with the M=O distances in the hydrates elongated by 0.016 – 0.027 Å, or by 0.047 Å in the case of Th^{IV}. The structures in Figure 10 demonstrate that "physisorption" hydrates are not bound only by ion-dipole interactions, with quotation marks used here to emphasize that there are clearly distinct M-OH_2 chemical bonds between the metal center and water. The hydrate structures indicate orbital-induced directional dative bonding that substantially affects the orientation of the H_2O ligands. This effect is

particularly obvious for dihydrates exhibiting the *Pr-type* structure with nearly linear O=M=O, where the angles $\alpha_{W\text{-}W}$ in Figure 10 are highly compressed from the value of 180° expected for a simple ion-dipole interaction and inter-ligand repulsion between adsorbed H_2O molecules.

Energies for "physisorption" of H_2O to MO_2, 1st hydration reaction (4a), and H_2O to $(H_2O)MO_2$, 2nd hydration reaction (4b), are plotted in Figure 11. Dative bonding decreases the charge on the metal in $(H_2O)MO_2$ relative to MO_2 such that the ion-dipole contribution and exothermicity of the 2nd hydration is slightly reduced, by less than 20%, relative to the energy of the 1st hydration. Also in accord with a contribution from an ion-dipole interaction, hydration is most exothermic for dipositive U^{VI}, intermediate for monopositive M^V, and least exothermic for neutral Th^{IV}. More interesting from a bonding perspective is the variation in hydration energies among the different M^V. Whereas f-block Pr^V, Pu^V, Am^V, U^V and Pa^V have 1st hydration energies in the range of -28 to -33 kcal/mol, those for d-block V^V, Nb^V and Ta^V are significantly more exothermic, in the range of -46 to -53 kcal/mol. Although NPA charges q(M) from NBOs are not actual physical parameters, they do reveal variations between metals. The charges q(M) for MO_2, plotted in Figure 11, are in the range of 2.4 to 2.9 for all of the M^V, except for V^V. For the actinides, the positive charge decreases across the series from Pa^V to Am^V, suggesting a corresponding increase in M=O bond covalency, in accord with a previous assessment.[105] The charges in MO_2 for M = Nb^V and Ta^V are similar to those for the actinides, while that for M = V^V is substantially less positive. Remarkably, the charge on vanadium in cation VO_2^+ (q(V) = +2.05) is much lower than on thorium in neutral ThO_2 (q(Th) = +2.50). The particularly large charge transfer from O to the metal center in V^V is indicative of especially enhanced V=O covalent bonding. Notably, hydration is markedly exothermic for V^V, which also has a particularly low positive charge on the metal center; this relationship is certainly not characteristic of a simple ion-dipole interaction between V^V and H_2O, but rather indicates substantial dative bonding.

As discussed above, the dihydrate structures indicate directional dative bonding, whereas hydration energies suggest that this bonding is greatest for V^V/Nb^V/Ta^V. Bond distances are another indicator of dative bonding. Distances d[M=O] in MO_2, plotted in Figure 11, exhibit trends characteristic of the corresponding metal ionic radii. Thus, the difference of -0.23 Å between the M=O distances for Pa^V (1.778 Å) and V^V (1.551 Å) is close to the difference of -0.26 Å between the radii of Pa^V and V^V (Table 3). Such correspondence suggests M=O bonds of comparable character for the MO_2 for the six M^V. In contrast, the M-OH_2 distances in $(H_2O)MO_2$ exhibit larger variations. These M-OH_2 distances are similar for Pr^V, U^V and Pa^V, but decrease by 0.46 Å between Pa^V and V^V. The bond distances, like hydration energies, thus indicate particularly substantial dative bonding, and resulting shorter metal-water bonds, in hydrates of V^V, Nb^V and Ta^V.

Conclusions

Transformation of a hydrated metal dioxide $(H_2O)_2MO_2$ to hydroxide $M(OH)_4$ entails no change in oxidation state or number of metal-oxygen bonds. Energetics for these transformations reflect relative stabilities of the four M-O bonds in the hydrate versus the four in the hydroxide. Addition of two H_2O to several MO_2 was examined by experiment to qualitatively assess these energies. The experimental results were initially taken to suggest two types of behavior: hydrate formation for M = Pr^V, U^V, Np^V, Am^V and V^V (as well as for M = U^{VI}); and hydroxide formation for M = Pa^V, Nb^V, and Ta^V (as well as for M = Th^{IV}). Notably, 4f-block $Pr^VO_2^+$ exhibits chemistry

also characteristic of 5f-block uranyl and later actinyls, whereas homologous $Pa^{V}O_2^+$ behaves like a heavy d-block transition metal dioxide.

Computed energies are in essential accord with experiment, except for the computational predictions that $(H_2O)VO(OH)_2^+$ is slightly more stable than $(H_2O)_2VO_2^+$, and $Nb(OH)_4^+$ is more stable than $(H_2O)NbO(OH)_2^+$. These predictions are considered valid, with experimentally observed H_2O elimination ascribed to de-hydrolysis and H_2O elimination from hydroxides, induced by acetone. The initial experimental assignments as $(H_2O)_2VO_2^+$ and $(H_2O)NbO(OH)_2^+$ were thus revised to $(H_2O)VO(OH)_2^+$ and $Nb(OH)_4^+$, in accord with the computational results. De-hydrolysis induced by acetone addition is a gas-phase phenomenon that is not generally expected in solution.

Computed structures indicate that PrO_2^+ and PaO_2^+ are linear actinyl-like species, which is ascribed to involvement of 4f (Pr) or 5f (Pa) orbitals in bonding. The resistance of PrO_2^+ to hydrolyze to $Pr(OH)_4^+$, and the low-symmetry structure of the latter, substantiate assignment of PrO_2^+ as *praseodymyl*, the first 4f *lanthanyl*. In contrast, exothermic hydrolysis of PaO_2^+ to $Pa(OH)_4^+$ with a high-symmetry T_d structure indicates characteristic d-block transition metal character in the hydroxide. Whereas the 4f *lanthanyl* PrO_2^+ and 5f actinyl UO_2^+ moieties are resistant to conversion to hydroxides, hydrated PaO_2^+ exothermically isomerizes to yield a tetrahedral hydroxide. Given that Th^{IV} is most susceptible to hydrolysis, Pa^{V} is identified as a bridge between the 6d-block transition elements, including Th, and the true 5f-block actinide elements that start with U. The structures of $Pu(OH)_4^+$ and $Pr(OH)_4^+$ are distinctive among the studied $M(OH)_4^+$, with imposition of a quasi-linear HO-M-OH linkage indicating participation of Pu 5f and Pr 4f orbitals in covalent bonding.

The results demonstrate utility of gas-phase reactivity to reveal and understand chemistry of d-block and f-block metals. Behavior such as hydrolysis of Pa^{V}, and contrasting hydration of uranyl, appear in both gas and solution phases. The gas-phase results show that this change across the actinide series can be traced to a shift from 6d-orbital bonding in Pa^{V} to 5f-orbital bonding in U^{V}, the latter being a central attribute of actinide chemistry. In view of the doubtful stability of oxidation state Pr^{V} in condensed phases, the present gas-phase results provide important insight into the essential nature of this species as *praseodymyl*, a genuine 4f-block *lanthanyl*.

Supporting Information

Complete citations for references 61 and 85; mass spectra showing formation of ions used for results in Figures 1 and 2; mass spectra as in Figures 1 and 2 but using different reaction times; PEPs for addition of water to bare MO_2 and hydrated $(H_2O)MO_2$ showing effect of solvation on hydration/hydrolysis; computed bond distances, vibrational frequencies, and NBO charges and populations; bond angles for species in Figure 7; optimized coordinates for each species on the PEPs.

Acknowledgements

This work was supported by the U.S. Department of Energy, Office of Science, Office of Basic Energy Sciences, Chemical Sciences, Geosciences, and Biosciences Division, Heavy Element Chemistry Program, at Lawrence Berkeley National Laboratory under Contract DE-AC02-05CH11231 (PDD, JKG), at The University of Alabama through Grant No. DE-SC0018921 (MV,

DAD), and at Argonne National Laboratory contract DE-AC02-06CH11357 (REW). D.A.D. thanks the Robert Ramsay Fund at The University of Alabama. Part of the computational work has been performed using the MSCF in the EMSL at PNNL. The EMSL is funded by the Office of Biological and Environmental Research in the U.S. Department of Energy.

Table 1. Products expected for addition of 1, 2 and 3 acetone (aco) molecules to different isomers of species with aggregate compositions *[MO_2 + 2H_2O]* and *[(aco)MO_2 + 2H_2O]*.[a,b]

Reactant[c]	***+ 1 aco***	***+ 2 aco***	***+ 3 aco***
[MO_2 + 2H_2O] ***M = V^V, Nb^V, Ta^V***			
[a] $(H_2O)_2MO_2$ (4)	(aco)$(H_2O)MO_2$ (4) + H_2O	$(aco)_2MO_2$ (4) + 2H_2O	$(aco)_3MO_2$ (5)[d] + 2H_2O
[b] $(H_2O)MO(OH)_2$ (4)	$(aco)MO(OH)_2$ (4) + H_2O	$(aco)_2MO(OH)_2$ (5) + H_2O	$(aco)_3MO(OH)_2$ (6) + H_2O
[c] $M(OH)_4$ (4)	$(aco)M(OH)_4$ (5)	$(aco)_2M(OH)_4$ (6)	-
[(aco)MO_2 + 2H_2O] ***M = Pr^V, Pa^V, U^V, Pu^V, Am^V***			
[a'] (aco)$(H_2O)_2MO_2$ (5)	$(aco)_2(H_2O)MO_2$ (5) + H_2O	$(aco)_3MO_2$ (5) + 2H_2O	$(aco)_4MO_2$ (6) + 2H_2O
[b'] (aco)$(H_2O)MO(OH)_2$ (5)	$(aco)_2MO(OH)_2$ (5) + H_2O	$(aco)_3MO(OH)_2$ (6) + H_2O	-
[c'] (aco)$M(OH)_4$ (5)	$(aco)_2M(OH)_4$ (6)	-	-

[a] "Expected" results assume aco displaces H_2O from hydrates but not from hydroxides.

[b] Coordination number (CN) is in parentheses.

[c] The M for which the reactant composition was employed in the experiments are as specified.

[d] Addition of another aco to yield $(aco)_4MO_2$ (CN = 6) is also feasible.

Table 2. Isomers resulting from addition of two H_2O to $M^VO_2^+$, initially inferred from reaction with acetone (***E***) and computationally predicted (***C***).

M	$(H_2O)_2MO_2$	$(H_2O)MO(OH)_2$	$M(OH)_4$
V^V	***E*[c]**	***C***	-
Nb^V	-	***E*[c]**	***C***
Ta^V	-	-	***E, C***
Pr^{Va}	***E, C***	-	-
Pa^{Va}	-	***E (minor)***	***E (major), C***
U^{Va}	***E, C***	-	-
Pu^{Va}	***E,C***	-	-
Am^{Va}	***E,C***	-	-

[a] Experiments were performed for species resulting from addition to $MO_2$of two H_2O and one acetone, *$[(aco)MO_2 + 2H_2O]$*, rather than *$[MO_2 + 2H_2O]$*.
[c] As discussed in the text, this initial assignment from experiments is considered incorrect; the species is instead assigned as that which is computationally predicted.

Table 3. Terminal observed complexes and coordination number (CN).

M^V	Major Species (CN)	Minor Species (CN)	IR[M^V][a]
V^V	$(aco)_3VO_2^+$ (5)	-	0.54 Å
Nb^V	$(aco)_2NbO(OH)_2^+$ (5)	$(aco)_3NbO(OH)_2^+$ (6)	0.69 Å
Ta^V	$(aco)Ta(OH)_4^+$ (5)	$(aco)_2Ta(OH)_4^+$ (6)	0.64 Å
Pr^V	$(aco)_3PrO_2^+$ (5)	-	~0.74 Å
Pa^V	$(aco)_2Pa(OH)_4^+$ (6) $(aco)_3PaO(OH)_2^+$ (6)	-	0.78
U^V	$(aco)_4UO_2^+$ (6)	-	0.76
Pu^V	$(aco)_3PuO_2^+$ (5)	$(aco)_4PuO_2^+$ (6)	0.74
Am^V	$(aco)_3AmO_2^+$ (5)	$(aco)_4AmO_2^+$ (6)	0.73

[a] Ionic radius (Å) from Shannon.[93] IR[Pr^V] roughly estimated as described in the text. IR[Am^V] estimated as ~0.01 Å smaller than IR[Pu^V].

Table 4. Energies (ΔH(298 K) in kcal/mol) for the species on the PEPs in Figures 3-6 computed at different levels of theory.[a]

MO_2	CCSD(T)[a]	$(H_2O)MO_2$	TS1	$MO(OH)_2$	TS2[b]	$(H_2O)MO(OH)_2$	TS3	$M(OH)_4$	$(H_2O)_2MO_2$	TS4
$^1ThO_2$	CBS	-20.7	-19.3	-58.9	NB	-79.3	-78.3	-121.6	-40.7	-39.5
$^1PaO_2^+$	CBS	-37.0	-7.2	-36.4	NB	-69.7	-43.6	-85.0	-70.0	-43.8
$^2UO_2^+$	CBS	-35.1	-0.6	-21.3	-21.2	-56.4[c]	-25.2 [c]	-47.4	-65.5	-36.5[c]
$^4PuO_2^+$	awT-DK	-35.4	6.6	-7.4	0.8	-42.9	0.2[d]	-25.8	-66.7	-27.8
$^5AmO_2^+$	awT-DK	-33.7	13.6	2.1	21.2	-31.0	6.2[d]	-17.1	-63.9	-20.2
$^1VO_2^+$	CBS	-55.1	-15.8	-60.4	NB	-114.3	-67.1	-102.1	-105.3	-71.9
$^1NbO_2^+$	CBS	-49.5	-16.8	-66.6	NB	-117.6	-83.6	-129.5	-95.3	-67.3
$^1TaO_2^+$	CBS	-58.8	-32.7	-88.4	NB	-145.3	-118.6	-172.1	-111.4	-88.4
$^1PrO_2^+$	CBS-DK	-31.5	12.8	1.9	4.2	-28.5	14.1	-1.9[e]	-59.5	-18.8
$^1UO_2^{2+}$	CBS	-66.5	-8.0	-36.2	-33.8	-93.5	-40.6	-70.8	-124.3	-68.6

[a] CCSD(T)/CBS using (a)V*n*Z(-PP) basis sets for Th, Pa, U, V, Nb and Ta; CCSD(T)/awT-DK: aug-cc-pVTZ-DK(H)/aug-cc-pwCVTZ-DK(O)/cc-pwCVTZ-DK3(Pu, Am); CCSD(T)/CBS-DK: aug-cc-pV*n*Z-DK(H)/aug-cc-pwCV*n*Z-DK(O)/cc-pwCV*n*Z-DK3(Pr); See text.

[b] TS2 is for rearrangement of OH moieties upon hydration of $MO(OH)_2$ to $(H_2O)MO(OH)_2$. NB = no barrier. For simplicity, TS2 is not included on the PEPs.

[c] CCSD(T)/aug-cc-pVTZ(H,O)/cc-pVTZ-PP(U) value.

[d] B3LYP/aug-cc-pVTZ(H,O)/Stuttgart basis & ECP-60(Pu,Am) value.

[e] CCSD(T)/aug-cc-pVTZ-DK(H)/aug-cc-pwCVTZ-DK(O)/cc-pwCVTZ-DK3(Pr) value.

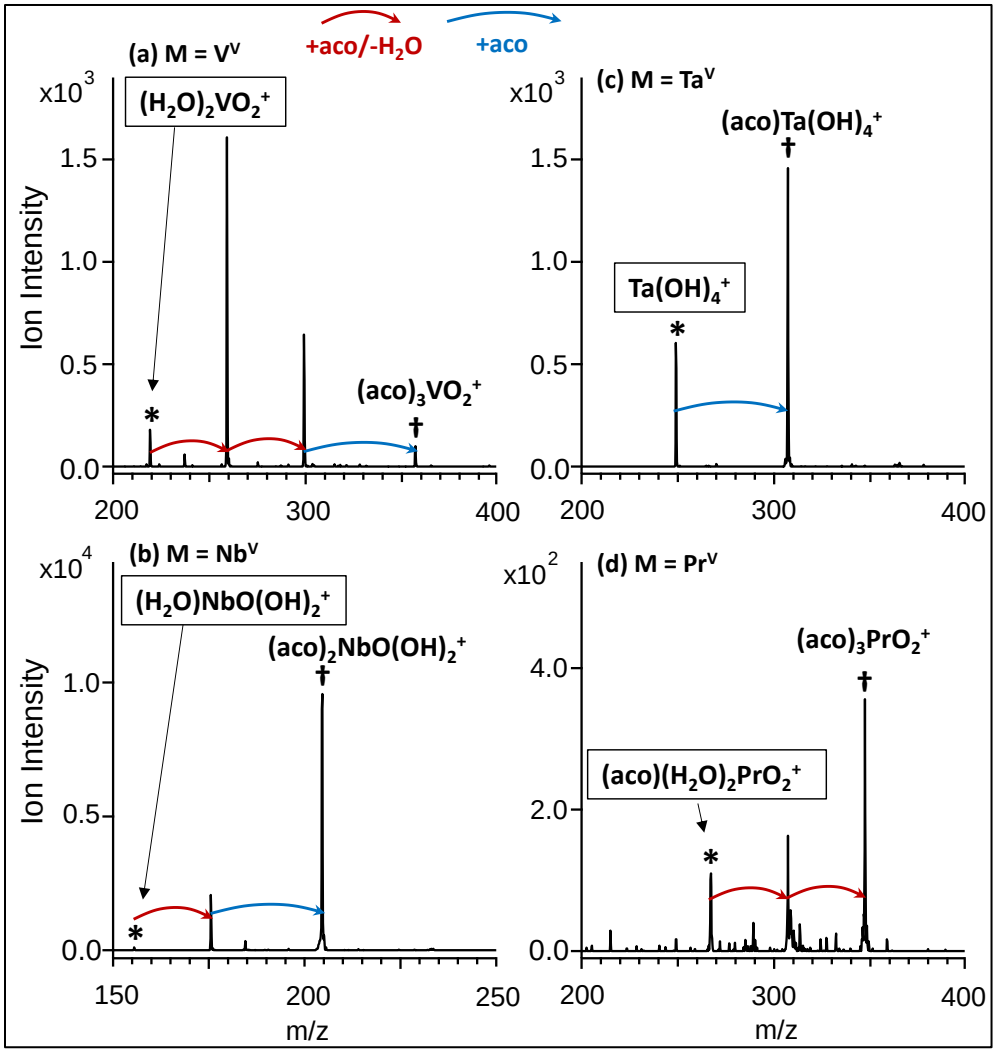

Figure 1. Mass spectra acquired after reaction with acetone (aco) for 0.5 s (2.0 sec for Pr at a lower aco pressure) of the species in the box (asterisked peak) for (a) M = V^V, (b) M = Nb^V, (c) M = Ta^V, and (d) M = Pr^V. Reaction pathways are replacement of H_2O by aco (red arrows) and addition of aco (blue arrows). The terminal product identified by a dagger has the indicated composition. The assigned isomer structures in this figure are based on the overly simplistic assumption that aco cannot displace H_2O from a hydroxide. The results for V^V and Nb^V were later revised as follows: the species labelled here as "$(H_2O)_2VO_2^+$" is actually $(H_2O)VO(OH)_2^+$, and "$(H_2O)NbO(OH)_2^+$" is actually $Nb(OH)_4^+$.

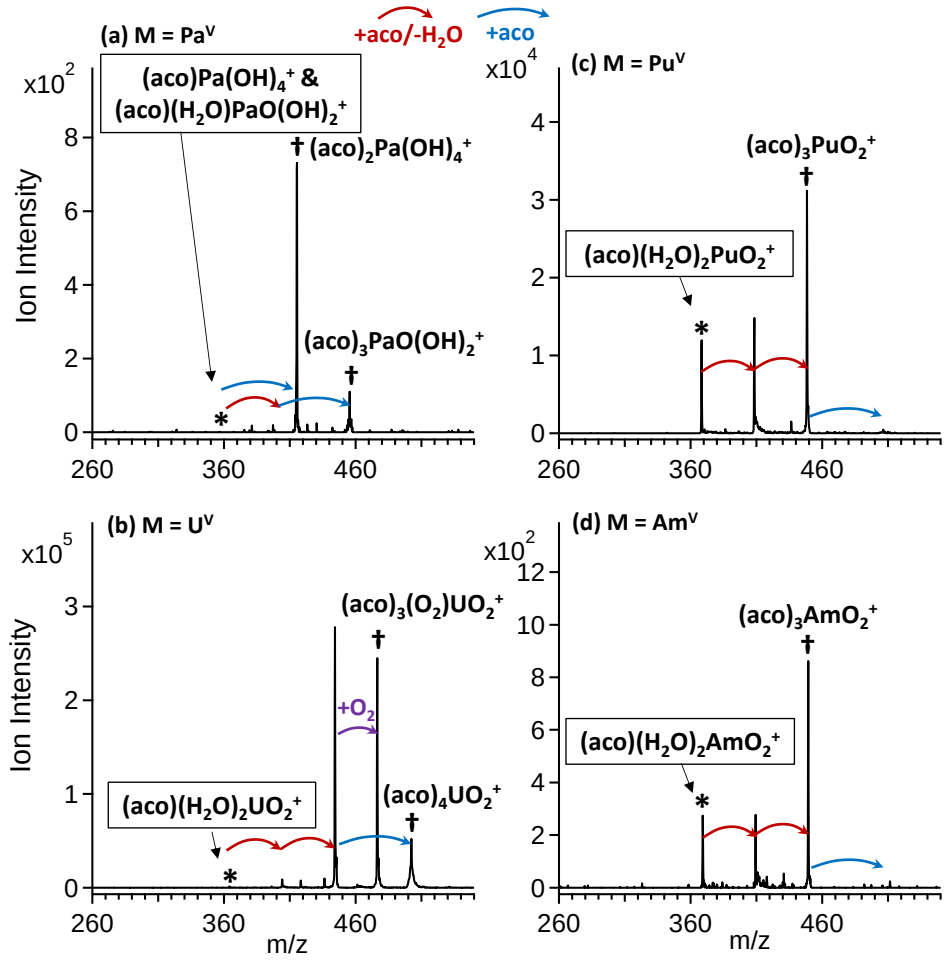

Figure 2. Mass spectra acquired after reaction with acetone (aco) for 0.5 s of the species in the box (asterisked peak) for (a) M = Pa^V, (b) M = U^V, (c) M = Pu^V, and (d) M = Am^V. Reaction pathways are replacement of H_2O by aco (red arrows) and addition of aco (blue arrows). Terminal product(s) identified by a dagger have the assigned composition. For M = Pa there are two precursors and terminal products. For M = Pu and Am there is indicated addition of a final aco to yield very minor $(aco)_4MO_2$. As in Figure 1, the assigned isomer structures are based on the simplistic assumption that aco cannot displace H_2O from a hydroxide, which is considered valid for these four M^V such that no changes to the indicated assignments were made.

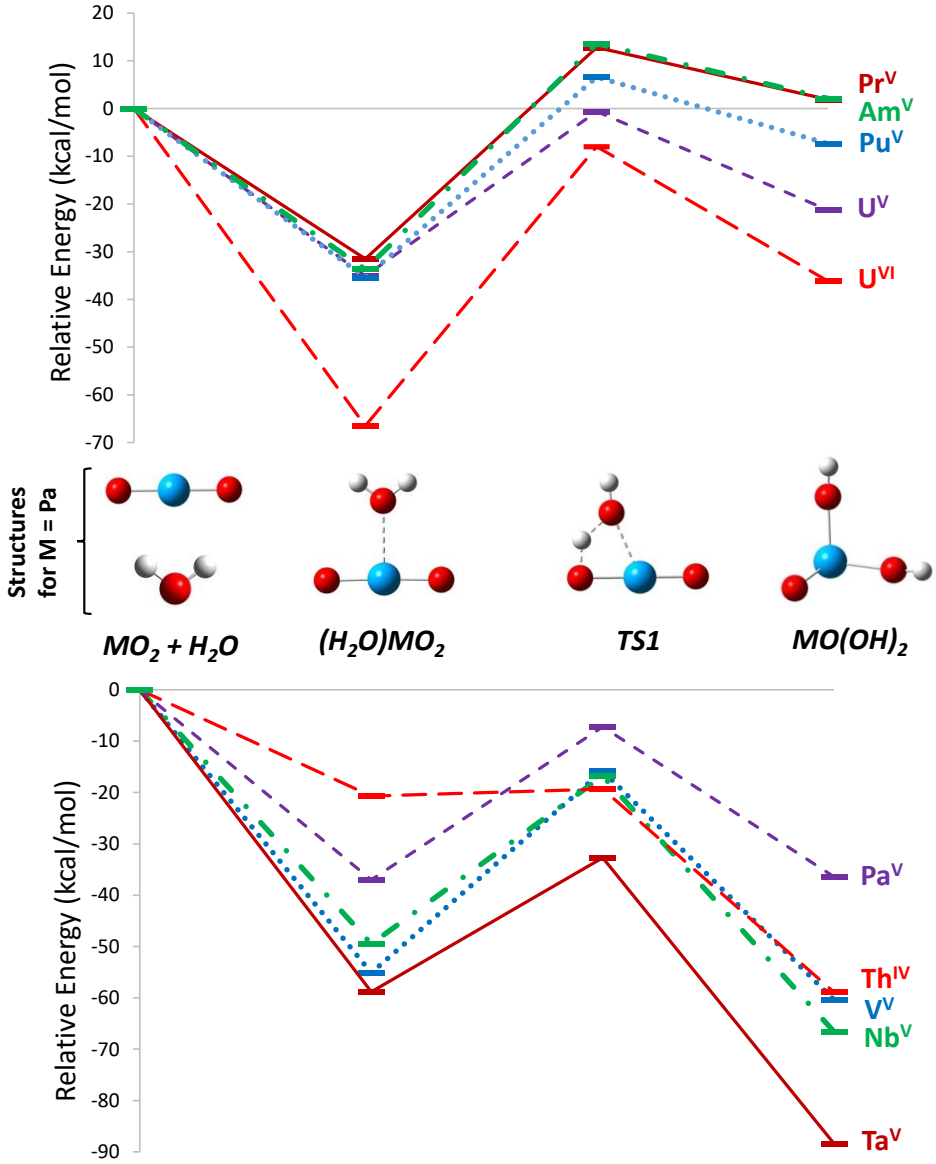

Figure 3. PEPs for addition of H_2O to MO_2 corresponding to reactions (4a) and (5a). The shown structures are for the specific case of M = Pa^V and are different for other M.

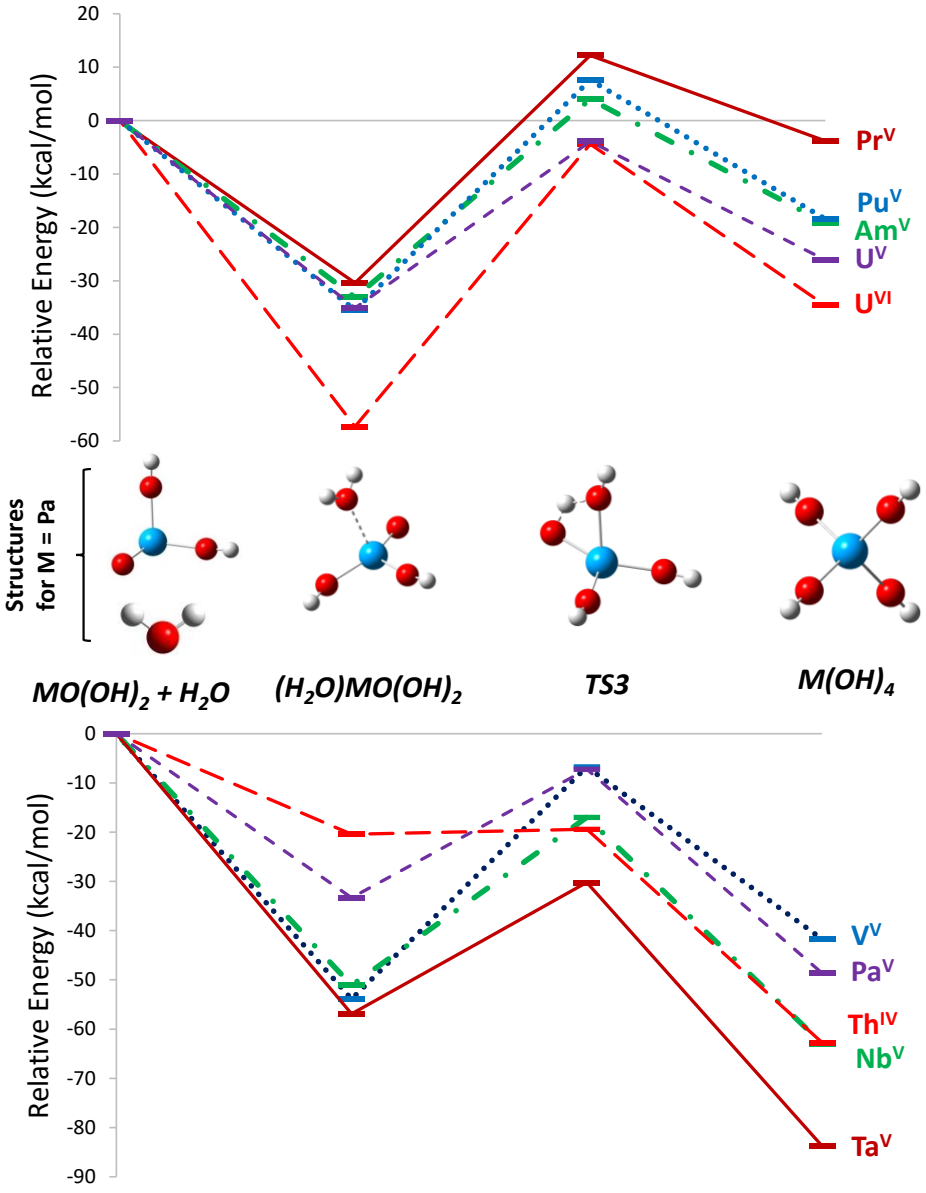

Figure 4. PEPs for addition of H_2O to $MO(OH)_2$ corresponding to reactions (5b) and (5c). The shown structures are for the specific case of M = Pa^V and are different for other M. Omitted for simplicity are the following TS2 barriers (in kcal/mol) for addition of H_2O to $MO(OH)_2$: Pr^V = 2.3; Am^V = 19.1; Pu^V = 8.2; U^V = 0.1; and U^{VI} = 2.5.

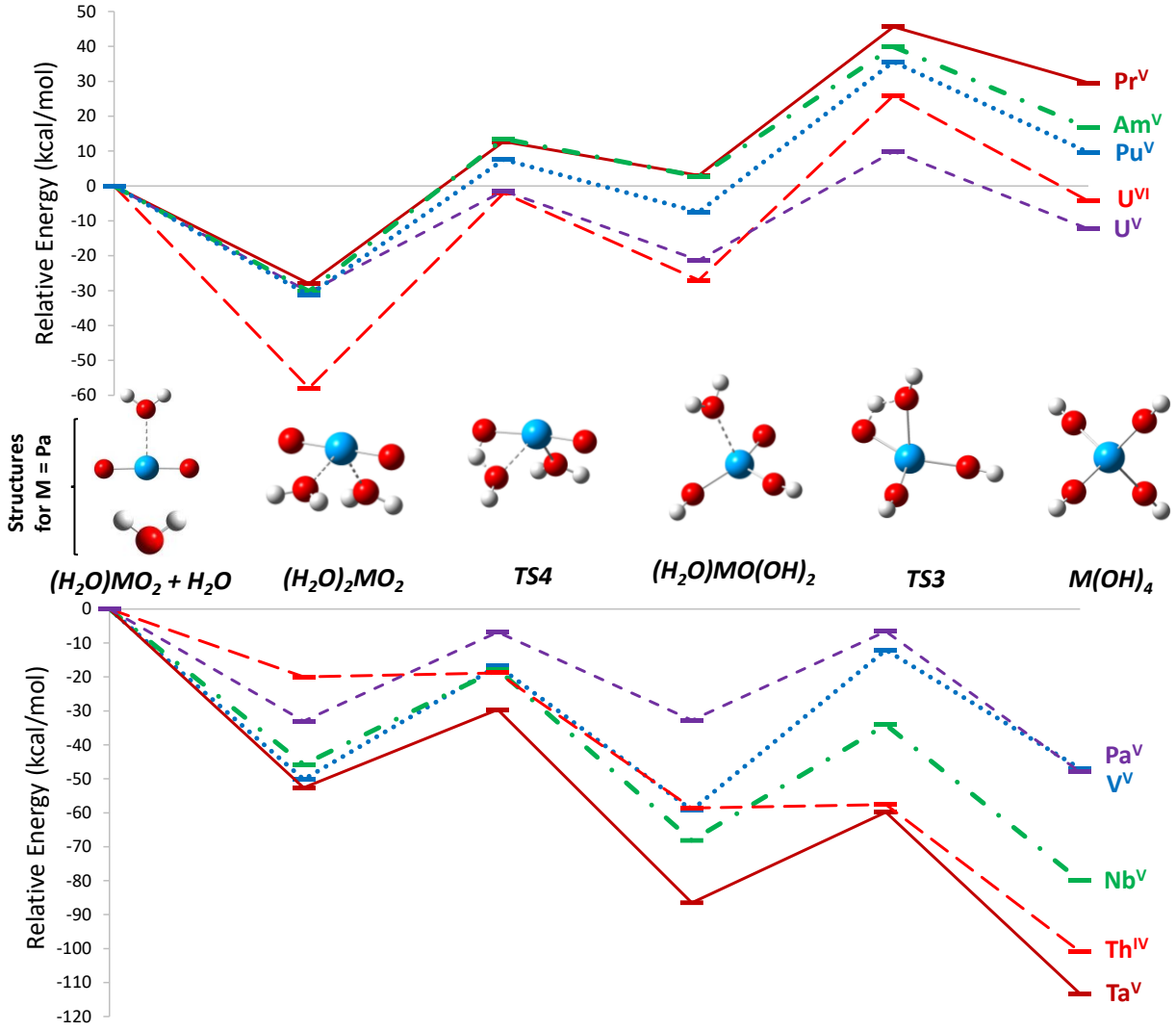

Figure 5. PEPs for addition of H_2O to $(H_2O)MO_2$ corresponding to reactions (4b), (4c) and (4d). The shown structures are for the specific case of M = Pa^V and are different for other M.

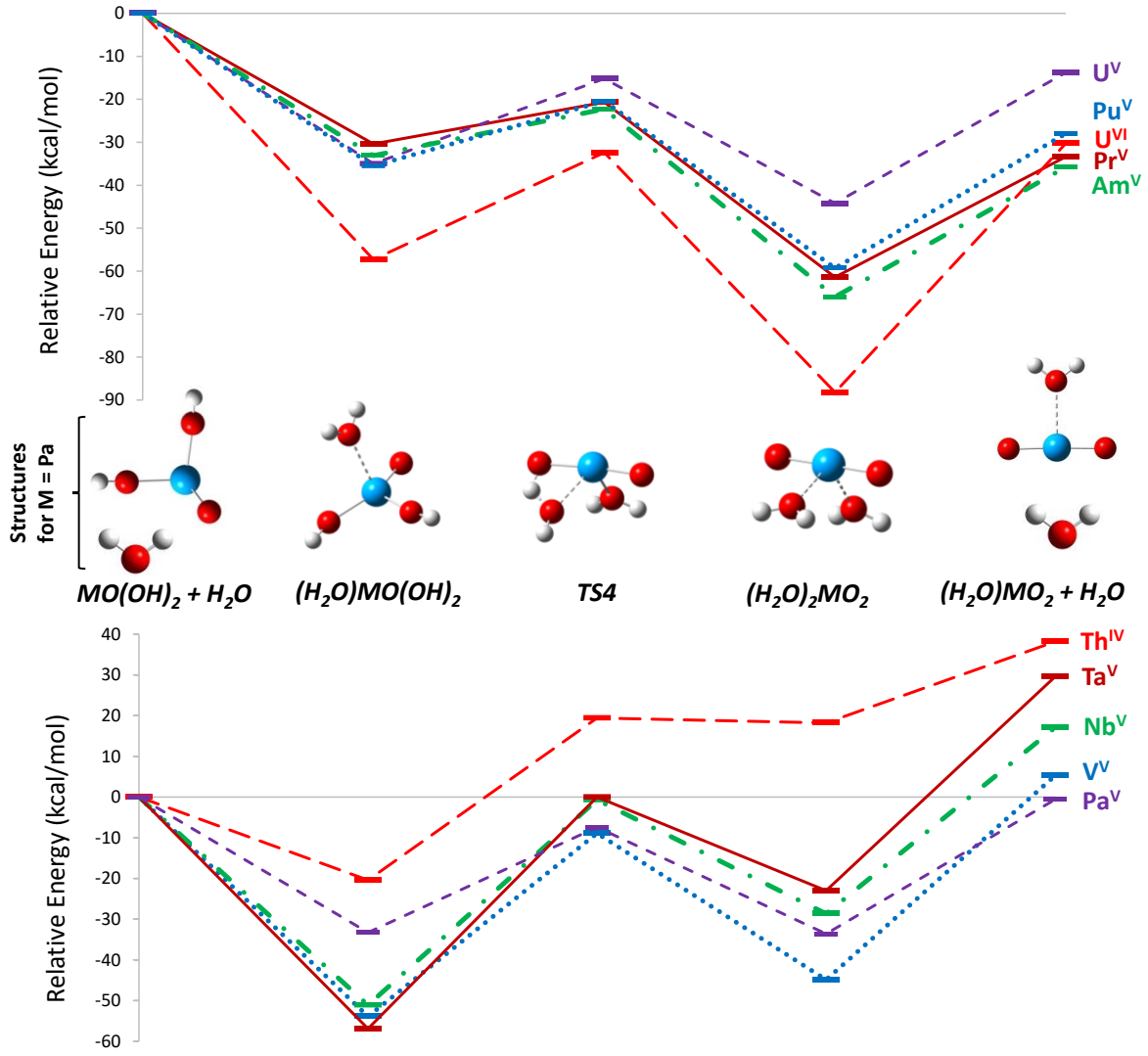

Figure 6. PEPs for addition of H_2O to $MO(OH)_2$ corresponding to reaction (5d). The shown structures are for the specific case of M = Pa^V and are different for other M. Omitted for simplicity are TS2 barriers for addition of H_2O to $MO(OH)_2$ as noted in Figure 4. The final step, elimination of H_2O from $(H_2O)_2MO_2$, elucidates the feasibility of de-hydrolysis and H_2O elimination by ligand addition to $MO(OH)_2$.

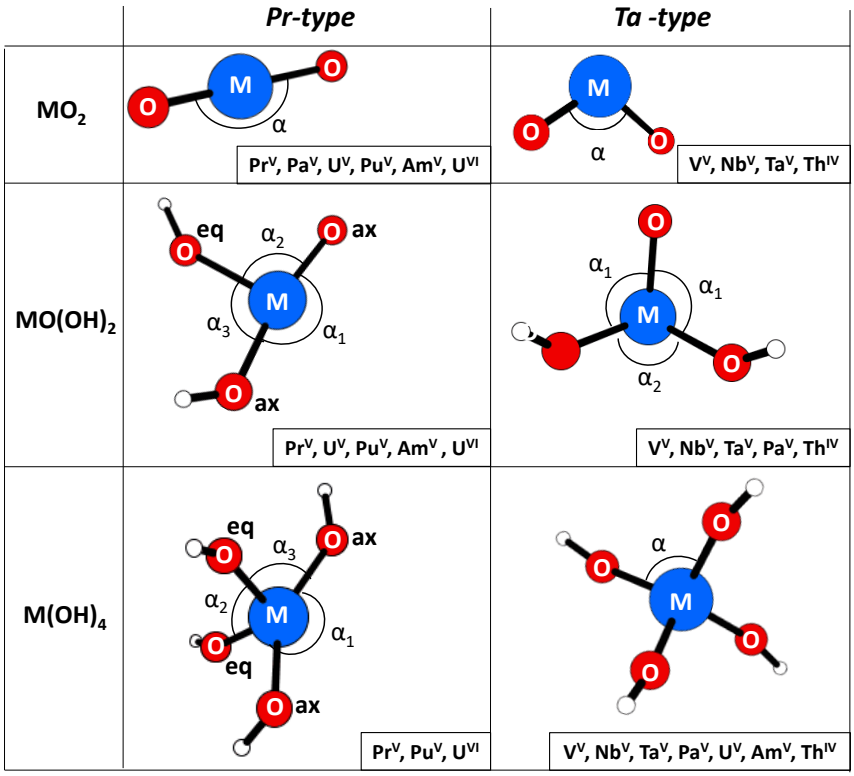

Figure 7. Prototypical structures (blue = M; red = O; grey = H): PrO_2^+, $PrO(OH)_2^+$ and $Pr(OH)_4^+$ (middle column / *Pr-type*); TaO_2^+, $TaO(OH)_2^+$ and $Ta(OH)_4^+$ (right column / *Ta-type*). Species represented by each structure type are in the inset boxes. Selected O atoms are identified as approximately axial (ax) or equatorial (eq). Values for angles are in Table S6.

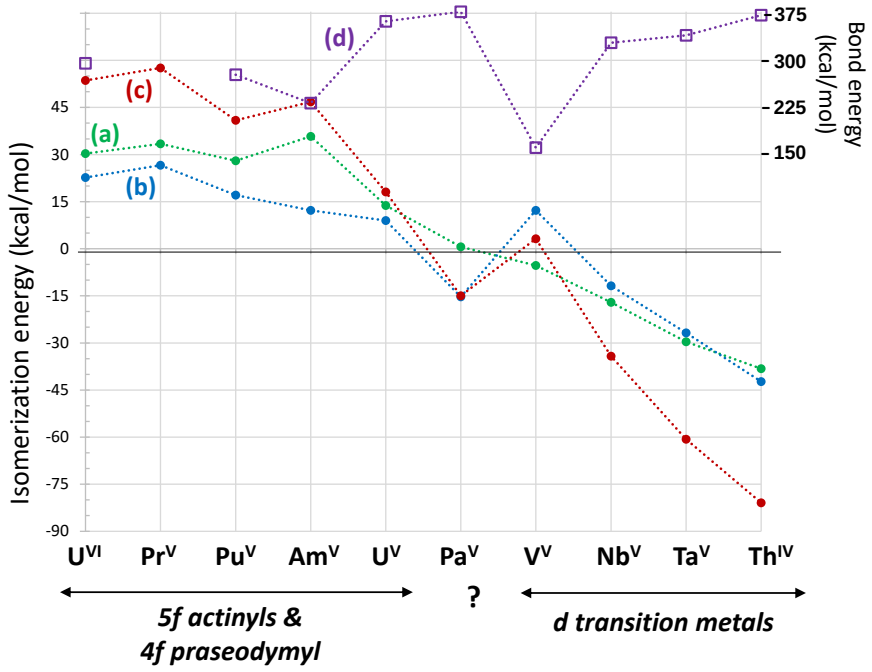

Figure 8. Isomerization energies (kcal/mol, left axis) for: (a) Reaction (10), $(H_2O)MO_2$ to $MO(OH)_2$ (green); (b) Reaction (11), $(H_2O)MO(OH)_2$ to $M(OH)_4$ (blue); and (c) Reaction (12), $(H_2O)_2MO_2$ to $M(OH)_4$ (red). Open squares (d) are energies (kcal/mol, right axis) for dissociation of MO_2 to M and 2O (from refs.[99, 100]; estimated IE[NbO_2] ≈ 7.4 eV; no value for Pr^V).

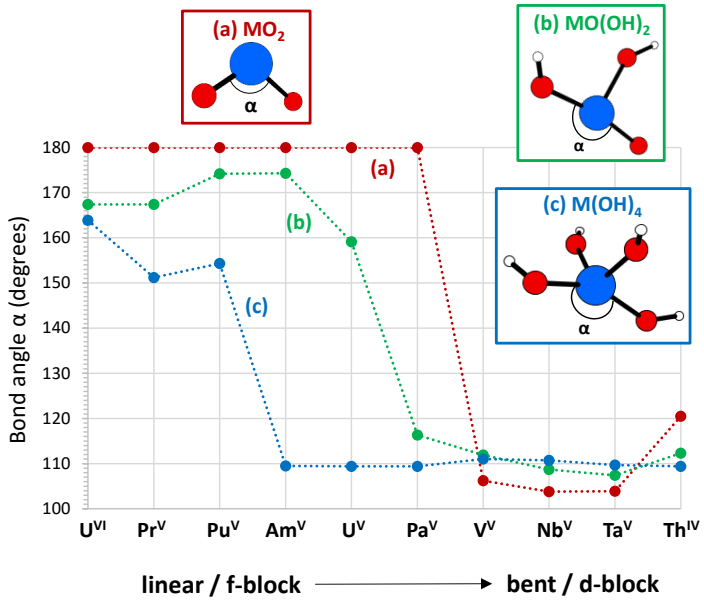

Figure 9. Selected bond angles: (a) O=M=O angle in MO_2; (b) largest O=M-O_{OH} angle in $MO(OH)_2$; (c) largest O_{OH}-M-O_{OH} angle in $M(OH)_4$. Linear structural moieties are associated with f-orbital bonding, whereas bent are associated with d-orbital bonding.

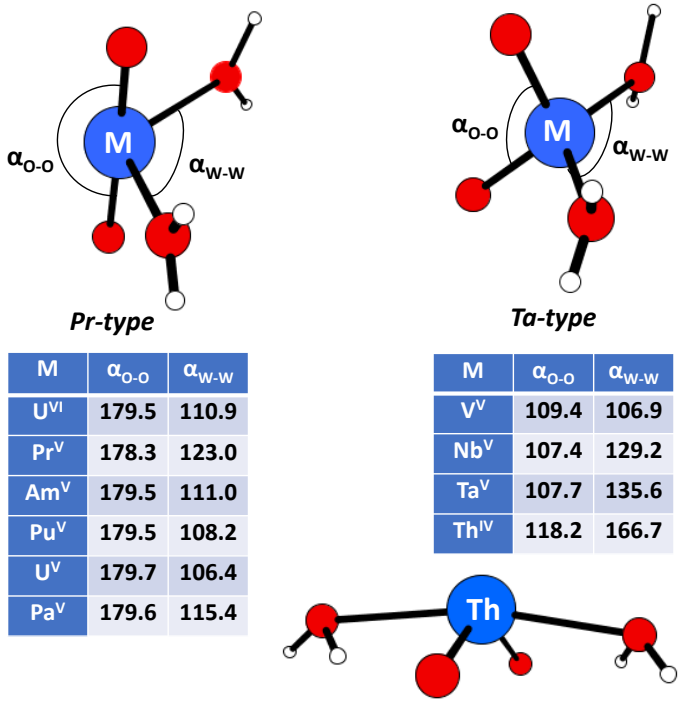

M	$\alpha_{O\text{-}O}$	$\alpha_{W\text{-}W}$
U^{VI}	179.5	110.9
Pr^{V}	178.3	123.0
Am^{V}	179.5	111.0
Pu^{V}	179.5	108.2
U^{V}	179.7	106.4
Pa^{V}	179.6	115.4

M	$\alpha_{O\text{-}O}$	$\alpha_{W\text{-}W}$
V^{V}	109.4	106.9
Nb^{V}	107.4	129.2
Ta^{V}	107.7	135.6
Th^{IV}	118.2	166.7

Figure 10. Two structure types for dihydrates $(H_2O)_2MO_2$, *Pr-type* with nearly linear MO_2, and *Ta-type* with highly bent MO_2. Selected bond angles (α in degrees) for the specific members of both structure types. The distinctive pyramidal-like structure of $(H_2O)_2ThO_2$ is shown.

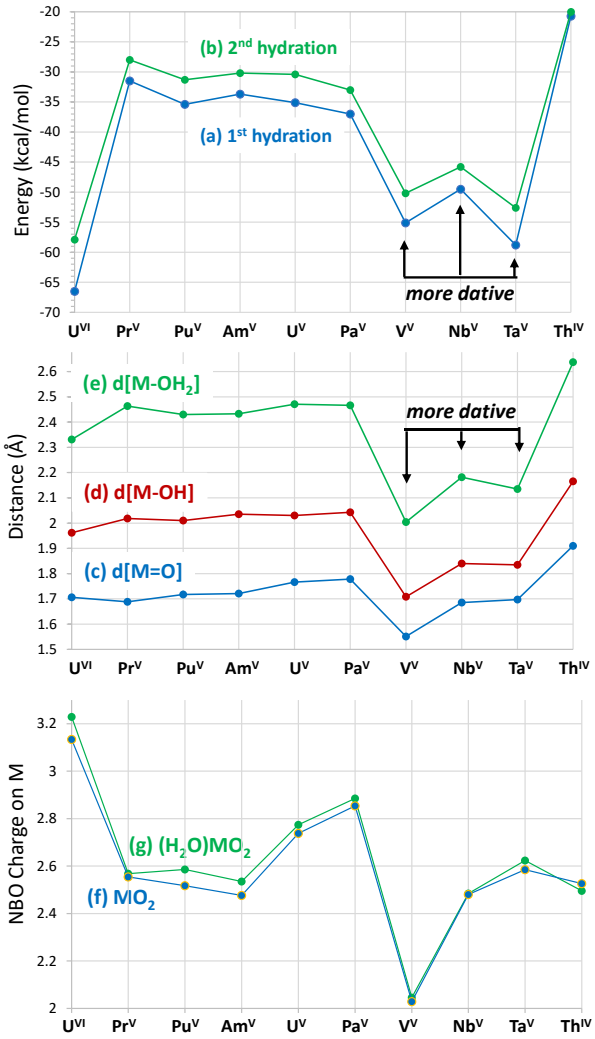

Figure 11. Top: Hydration energy for addition of H_2O to (a) MO_2 (1st hydration), and (b) $(H_2O)MO_2$ (2nd hydration). Middle: Bond distance for (c) M-O in MO_2, (d) M-OH in $M(OH)_4$, and (e) M-OH_2 in $(H_2O)MO_2$. Bottom: NBO charge on M in (f) MO_2, and (g) $(H_2O)MO_2$. Energies and distances suggest enhanced dative bonding in hydrates of VO_2^+, NbO_2^+ and TaO_2^+.

References

1. Dyrssen, D.; Sekine, T., Mononuclear Hydrolysis of Vanadium(V). *Acta Chem Scand* **1961,** *15* (6), 1399-1400.
2. Yamada, S.; Funahashi, S.; Tanaka, M., Hydrolysis of Pervanadyl Ion. *J Inorg Nucl Chem* **1975,** *37* (3), 835-837.
3. Borgen, O.; Mahmoud, M. R.; Skauvik, I., Reinvestigation of Hydrolysis of Pentavalent Vanadium. *Acta Chem Scand A* **1977,** *31* (5), 329-339.
4. Overbeek, R. A.; Bosma, E. J.; deBlauw, D. W. H.; vanDillen, A. J.; Bruil, H. G.; Geus, J. W., The Hydrolysis Behavior of Vanadium Species in Aqueous Solutions and Their Adsorption on Alumina, Silica and Titania Surfaces. *Appl Catal A-Gen* **1997,** *163* (1-2), 129-144.
5. Jiang, Z.; Klyukin, K.; Alexandrov, V., Structure, Hydrolysis, and Diffusion of Aqueous Vanadium Ions from Car-Parrinello Molecular Dynamics. *J Chem Phys* **2016,** *145* (11), 114303.
6. Etxebarria, N.; Fernandez, L. A.; Madariaga, J. M., On the Hydrolysis of Niobium(V) and Tantalum(V) in 3-mol dm(-3) KCl at 25-Degrees-C .1. Construction of a Thermodynamic Model for Nb-V. *J Chem Soc Dalton* **1994,** (20), 3055-3059.
7. Hill, J. O.; Worsley, I. G.; Hepler, L. G., Thermochemistry and Oxidation Potentials of Vanadium, Niobium, and Tantalum. *Chem Rev* **1971,** *71* (1), 127-137.
8. Aveston, J.; Johnson, J. S., Hydrolysis of Tantalum(V) - Equilibrium Ultracentrifugation & Raman Spectra of Potassium Tantalate. *Inorg Chem* **1964,** *3* (7), 1051-1053.
9. La Naour, C.; Roques, J.; Den Auwer, C.; Moisy, P.; Aupiais, J., Protactinium(V) in Aqueous Solution: A Light Actinide Without Actinyl Moiety. *Radiochim Acta* **2019,** *107* (9-11), 979-991.
10. Wilson, R. E.; De Sio, S.; Vallet, V., Structural and Electronic Properties of Fluoride Complexes of Nb-V, Ta-V, and Pa-V: The Influence of Relativistic Effects on Group V Elements. *Eur J Inorg Chem* **2016,** (35), 5467-5476.
11. Wilson, R. E.; De Sio, S.; Vallet, V., Protactinium and the Intersection of Actinide and Transition Metal Chemistry. *Nat Commun* **2018,** *9*.
12. Wadt, W. R., Why UO2(2+) is Linear and Isoelectronic ThO2 Is Bent. *J Am Chem Soc* **1981,** *103* (20), 6053-6057.
13. Kaupp, M., On the Relation Between Pi Bonding, Electronegativity, and Bond Angles in High-Valent Transition Metal Complexes. *Chem-Eur J* **1999,** *5* (12), 3631-3643.
14. Straka, M.; Hrobarik, P.; Kaupp, M., Understanding Structure and Bonding in Early Actinide 6d(0)5f(0) MX6q (M = Th-Np; X = H, F) Complexes in Comparison with Their Transition Metal 5d(0) Analogues. *J Am Chem Soc* **2005,** *127* (8), 2591-2599.
15. Quemet, A.; Brennetot, R.; Salpin, J. Y.; Cimas, A.; Marsden, C.; Tortajada, J.; Vitorge, P., How Can f-Block Monocations Behave as Monocations of d-Block Transition Metals? *Eur J Inorg Chem* **2012,** (22), 3551-3555.
16. Wills, J. M.; Eriksson, O., Crystal-Structure Stabilities and Electronic-Structure for the Light Actinides Th, Pa, and U. *Phys Rev B* **1992,** *45* (24), 13879-13890.
17. Dumas, T.; Guillaumont, D.; Fillaux, C.; Scheinost, A.; Moisy, P.; Petit, S.; Shuh, D. K.; Tyliszczak, T.; Den Auwer, C., The Nature of Chemical Bonding in Actinide and Lanthanide Ferrocyanides Determined by X-ray Absorption Spectroscopy and Density Functional Theory. *Phys Chem Chem Phys* **2016,** *18* (4), 2887-2895.
18. Wu, Q. Y.; Wang, C. Z.; Lan, J. H.; Xiao, C. L.; Wang, X. K.; Zhao, Y. L.; Chai, Z. F.; Shi, W. Q., Theoretical Investigation on Multiple Bonds in Terminal Actinide Nitride Complexes. *Inorg Chem* **2014,** *53* (18), 9607-9614.

19. Polinski, M. J.; Garner, E. B.; Maurice, R.; Planas, N.; Stritzinger, J. T.; Parker, T. G.; Cross, J. N.; Green, T. D.; Alekseev, E. V.; Van Cleve, S. M., et al., Unusual Structure, Bonding and Properties in a Californium Borate. *Nat Chem* **2014,** *6* (5), 387-392.
20. Petit, L.; Adamo, C.; Maldivi, P., Toward a Clear-Cut Vision on the Origin of 2,6-di(1,2,4-triazin-3-yl)pyridine Selectivity for Trivalent Actinides: Insights From Theory. *Inorg Chem* **2006,** *45* (21), 8517-8522.
21. Berryman, V. E. J.; Whalley, Z. J.; Shephard, J. J.; Ochiai, T.; Price, A. N.; Arnold, P. L.; Parsons, S.; Kaltsoyannis, N., Computational Analysis of M-O Covalency in M(OC6H5)(4) (M = Ti, Zr, Hf, Ce, Th, U). *Dalton T* **2019,** *48* (9), 2939-2947.
22. Cox, R. M.; Citir, M.; Armentrout, P. B.; Battey, S. R.; Peterson, K. A., Bond energies of ThO+ and ThC+: A guided ion beam and quantum chemical investigation of the reactions of thorium cation with O-2 and CO. *J Chem Phys* **2016,** *144* (18), 184309.
23. Brewer, L., Energies of Electronic Configurations of Lanthanide and Actinide Neutral Atoms. *J Opt Soc Am* **1971,** *61* (8), 1101-1111.
24. Santos, M.; de Matos, A. P.; Marçalo, J.; Gibson, J. K.; Haire, R. G.; Tyagi, R.; Pitzer, R. M., Oxidation of Gas-Phase Protactinium Ions, Pa+ and Pa2+: Formation and Properties of PaO22+(g), Protactinyl. *J Phys Chem A* **2006,** *110* (17), 5751-5759.
25. Zhang, Q. N.; Hu, S. X.; Qu, H.; Su, J.; Wang, G. J.; Lu, J. B.; Chen, M. H.; Zhou, M. F.; Li, J., Pentavalent Lanthanide Compounds: Formation and Characterization of Praseodymium(V) Oxides. *Angew Chem Int Edit* **2016,** *55* (24), 6896-6900.
26. Hu, S. X.; Jian, J. W.; Su, J.; Wu, X.; Li, J.; Zhou, M. F., Pentavalent Lanthanide Nitride-Oxides: NPrO and NPrO- Complexes with N Equivalent to Pr Triple Bonds. *Chem Sci* **2017,** *8* (5), 4035-4043.
27. Monteiro, B.; Bandeira, N. A. G.; Lourenço, C.; Lucena, A. F.; Carretas, J. M.; Gibson, J. K.; Marçalo, J., Chemical Evidence of the Stability of Praseodymium(v) in Gas-Phase Oxide Nitrate Complexes. *Chem Commun* **2019,** *55* (94), 14139-14142.
28. Ionova, G. V.; Pershina, V. G.; Spitsyn, V. I., Effect of Relativistic Effects on Properties of Compounds of Heavy-Elements. *Zh Neorg Khim* **1983,** *28* (12), 3107-3112.
29. Heinemann, C.; Cornehl, H. H.; Schroder, D.; Dolg, M.; Schwarz, H., The CeO2+ Cation: Gas-Phase Reactivity and Electronic Structure. *Inorg Chem* **1996,** *35* (9), 2463-2475.
30. Jian, T.; Dau, P. D.; Shuh, D. K.; Vasiliu, M.; Dixon, D. A.; Peterson, K. A.; Gibson, J. K., Activation of Water by Pentavalent Actinide Dioxide Cations: Characteristic Curium Revealed by a Reactivity Turn after Americium. *Inorg Chem* **2019,** *58* (20), 14005-14014.
31. Dau, P. D.; Vasiliu, M.; Peterson, K. A.; Dixon, D. A.; Gibson, J. K., Remarkably High Stability of Late Actinide Dioxide Cations: Extending Chemistry to Pentavalent Berkelium and Californium. *Chem-Eur J* **2017,** *23* (68), 17369-17378.
32. Johnson, J. R. T.; Panas, I., Hydrolysis on Transition Metal Oxide Clusters and the Stabilities of M-O-M Bridges. *Inorg Chem* **2000,** *39* (15), 3192-3204.
33. Johnson, J. R. T.; Panas, I., Water Adsorption and Hydrolysis on Molecular Transition Metal Oxides and Oxyhydroxides. *Inorg Chem* **2000,** *39* (15), 3181-3191.
34. Zavras, A.; Khairallah, G. N.; Krstic, M.; Girod, M.; Daly, S.; Antoine, R.; Maitre, P.; Mulder, R. J.; Alexander, S. A.; Bonacic-Koutecky, V., et al., Ligand-Induced Substrate Steering and Reshaping of [Ag-2(H)](+) Scaffold for Selective CO2 Extrusion from Formic Acid. *Nat Commun* **2016,** *7*.
35. Dau, P. D.; Wilson, R. E.; Gibson, J. K., Elucidating Protactinium Hydrolysis: The Relative Stabilities of PaO2(H2O)(+) and PaO(OH)(2)(+). *Inorg Chem* **2015,** *54* (15), 7474-7480.
36. Gong, Y.; Hu, H. S.; Rao, L. F.; Li, J.; Gibson, J. K., Experimental and Theoretical Studies on the Fragmentation of Gas-Phase Uranyl-, Neptunyl-, and Plutonyl-Diglycolamide Complexes. *J Phys Chem A* **2013,** *117* (40), 10544-10550.

37. Rios, D.; Rutkowski, P. X.; Shuh, D. K.; Bray, T. H.; Gibson, J. K.; Van Stipdonk, M. J., Electron Transfer Dissociation of Dipositive Uranyl and Plutonyl Coordination Complexes. *J Mass Spectrom* **2011,** *46* (12), 1247-1254.
38. Wilson, R. E., Retrieval and Purification of an Aged Pa-231 Source from its Decay Daughters. *Radiochim Acta* **2014,** *102* (6), 505-511.
39. De Sio, S. M.; Wilson, R. E., Structural and Spectroscopic Studies of Fluoroprotactinates. *Inorg Chem* **2014,** *53* (3), 1750-1755.
40. Gronert, S., Estimation of Effective Ion Temperatures in a Quadrupole Ion Trap. *J Am Soc Mass Spectr* **1998,** *9* (8), 845-848.
41. Rutkowski, P. X.; Michelini, M. C.; Bray, T. H.; Russo, N.; Marçalo, J.; Gibson, J. K., Hydration of Gas-Phase Ytterbium Ion Complexes Studied by Experiment and Theory. *Theor Chem Acc* **2011,** *129* (3-5), 575-592.
42. Rios, D.; Michelini, M. C.; Lucena, A. F.; Marçalo, J.; Bray, T. H.; Gibson, J. K., Gas-Phase Uranyl, Neptunyl, and Plutonyl: Hydration and Oxidation Studied by Experiment and Theory. *Inorg Chem* **2012,** *51* (12), 6603-6614.
43. Rios, D.; Micheini, M. D.; Lucena, A. F.; Marçalo, J.; Gibson, J. K., On the Origins of Faster Oxo Exchange for Uranyl(V) versus Plutonyl(V). *J Am Chem Soc* **2012,** *134* (37), 15488-15496.
44. Parr, R. G.; Yang, W., *Density-Functional Theory of Atoms and Molecules*. Oxford University Press: New York, 1989.
45. Becke, A. D., Density-Functional Thermochemistry .3. The Role of Exact Exchange. *J Chem Phys* **1993,** *98* (7), 5648-5652.
46. Lee, C. T.; Yang, W. T.; Parr, R. G., Development of the Colle-Salvetti Correlation-Energy Formula into a Functional of the Electron-Density. *Phys Rev B* **1988,** *37* (2), 785-789.
47. Dunning, T. H., Gaussian-Basis Sets for Use in Correlated Molecular Calculations .1. The Atoms Boron through Neon and Hydrogen. *J Chem Phys* **1989,** *90* (2), 1007-1023.
48. Kendall, R. A.; Dunning, T. H.; Harrison, R. J., Electron-Affinities of the 1st-Row Atoms Revisited - Systematic Basis-Sets and Wave-Functions. *J Chem Phys* **1992,** *96* (9), 6796-6806.
49. Peterson, K. A., Correlation Consistent Basis Sets for Actinides. I. The Th and U Atoms. *J Chem Phys* **2015,** *142* (7), 074105.
50. Vasiliu, M.; Peterson, K. A.; Gibson, J. K.; Dixon, D. A., Reliable Potential Energy Surfaces for the Reactions of H2O with ThO2, PaO2+, UO22+, and UO2+. *J Phys Chem A* **2015,** *119* (46), 11422-11431.
51. Dolg, M.; Cao, X. Y., Accurate Relativistic Small-Core Pseudopotentials for Actinides. Energy Adjustment for Uranium and First Applications to Uranium Hydride. *J Phys Chem A* **2009,** *113* (45), 12573-12581.
52. Weigand, A.; Cao, X. Y.; Hangele, T.; Dolg, M., Relativistic Small-Core Pseudopotentials for Actinium, Thorium, and Protactinium. *J Phys Chem A* **2014,** *118* (13), 2519-2530.
53. Kuchle, W.; Dolg, M.; Stoll, H.; Preuss, H., Energy-Adjusted Pseudopotentials for the Actinides - Parameter Sets and Test Calculations for Thorium and Thorium Monoxide. *J Chem Phys* **1994,** *100* (10), 7535-7542.
54. Cao, X. Y.; Dolg, M., Segmented Contraction Scheme for Small-Core Actinide Pseudopotential Basis Sets. *J Mol Struc-Theochem* **2004,** *673* (1-3), 203-209.
55. Cao, X. Y.; Dolg, M.; Stoll, H., Valence Basis Sets for Relativistic Energy-Consistent Small-Core Actinide Pseudopotentials. *J Chem Phys* **2003,** *118* (2), 487-496.
56. Dolg, M.; Stoll, H.; Preuss, H., Energy-Adjusted Abinitio Pseudopotentials for the Rare-Earth Elements. *J Chem Phys* **1989,** *90* (3), 1730-1734.
57. Cao, X. Y.; Dolg, M., Valence Basis Sets for Relativistic Energy-Consistent Small-Core Lanthanide Pseudopotentials. *J Chem Phys* **2001,** *115* (16), 7348-7355.

58. Li, S. G.; Hennigan, J. M.; Dixon, D. A.; Peterson, K. A., Accurate Thermochemistry for Transition Metal Oxide Clusters. *J Phys Chem A* **2009,** *113* (27), 7861-7877.
59. Figgen, D.; Peterson, K. A.; Dolg, M.; Stoll, H., Energy-Consistent Pseudopotentials and Correlation Consistent Basis Sets for the 5d Elements Hf-Pt. *J Chem Phys* **2009,** *130* (16).
60. Peterson, K. A.; Figgen, D.; Dolg, M.; Stoll, H., Energy-Consistent Relativistic Pseudopotentials and Correlation Consistent Basis Sets for the 4d Elements Y-Pd. *J Chem Phys* **2007,** *126* (12), 124101.
61. Frisch, M. J.; Trucks, G. W.; Schlegel, H. B.; Scuseria, G. E.; Robb, M. A.; Cheeseman, J. R.; Scalmani, G.; Barone, V.; Petersson, G. A.; Nakatsuji, H., et al. *Gaussian 16, Revision A.03*, Wallingford, CT, 2016.
62. Purvis, G. D.; Bartlett, R. J., A Full Coupled-Cluster Singles and Doubles Model - the Inclusion of Disconnected Triples. *J Chem Phys* **1982,** *76* (4), 1910-1918.
63. Raghavachari, K.; Trucks, G. W.; Pople, J. A.; Headgordon, M., A 5th-Order Perturbation Comparison of Electron Correlation Theories. *Chem Phys Lett* **1989,** *157* (6), 479-483.
64. Watts, J. D.; Gauss, J.; Bartlett, R. J., Coupled-Cluster Methods with Noniterative Triple Excitations for Restricted Open-Shell Hartree-Fock and Other General Single Determinant Reference Functions - Energies and Analytical Gradients. *J Chem Phys* **1993,** *98* (11), 8718-8733.
65. Bartlett, R. J.; Musial, M., Coupled-Cluster Theory in Quantum Chemistry. *Rev Mod Phys* **2007,** *79* (1), 291-352.
66. Feller, D.; Peterson, K. A.; Hill, J. G., On the effectiveness of CCSD(T) Complete Basis Set Extrapolations for Atomization Energies. *J Chem Phys* **2011,** *135* (4).
67. Peterson, K. A.; Woon, D. E.; Dunning, T. H., Benchmark Calculations with Correlated Molecular Wave-Functions .4. The Classical Barrier Height of the H+H-2-]H-2+H Reaction. *J Chem Phys* **1994,** *100* (10), 7410-7415.
68. Douglas, M.; Kroll, N. M., Quantum Electrodynamical Corrections to Fine-Structure of Helium. *Ann Phys-New York* **1974,** *82* (1), 89-155.
69. Jansen, G.; Hess, B. A., Revision of the Douglas-Kroll Transformation. *Phys Rev A* **1989,** *39* (11), 6016-6017.
70. Wolf, A.; Reiher, M.; Hess, B. A., The Generalized Douglas-Kroll Transformation. *J Chem Phys* **2002,** *117* (20), 9215-9226.
71. de Jong, W. A.; Harrison, R. J.; Dixon, D. A., Parallel Douglas-Kroll Energy and Gradients in NWChem: Estimating Scalar Relativistic Effects Using Douglas-Kroll Contracted Basis Sets. *J Chem Phys* **2001,** *114* (1), 48-53.
72. Peterson, K. A.; Dunning, T. H., Accurate Correlation Consistent Basis Sets for Molecular Core-Valence Correlation Effects: The Second Row Atoms Al-Ar, and the First Row Atoms B-Ne Revisited. *J Chem Phys* **2002,** *117* (23), 10548-10560.
73. Feng, R. L.; Peterson, K. A., Correlation Consistent Basis Sets for Actinides. II. The Atoms Ac and Np-Lr. *J Chem Phys* **2017,** *147* (8).
74. Lu, Q.; Peterson, K. A., Correlation Consistent Basis Sets for Lanthanides: The Atoms La-Lu. *J Chem Phys* **2016,** *145* (5), 054111.
75. Fang, Z. T.; Vasiliu, M.; Peterson, K. A.; Dixon, D. A., Prediction of Bond Dissociation Energies/Heats of Formation for Diatomic Transition Metal Compounds: CCSD(T) Works. *J Chem Theory Comput* **2017,** *13* (3), 1057-1066.
76. Fang, Z. T.; Both, J.; Li, S. G.; Yue, S. W.; Apra, E.; Keceli, M.; Wagner, A. F.; Dixon, D. A., Benchmark Calculations of Energetic Properties of Groups 4 and 6 Transition Metal Oxide Nanoclusters Including Comparison to Density Functional Theory. *J Chem Theory Comput* **2016,** *12* (8), 3689-3710.
77. Fang, Z. T.; Lee, Z.; Peterson, K. A.; Dixon, D. A., Use of Improved Orbitals for CCSD(T) Calculations for Predicting Heats of Formation of Group IV and Group VI Metal Oxide Monomers and Dimers and UCl6. *J Chem Theory Comput* **2016,** *12* (8), 3583-3592.

78. Perdew, J. P.; Wang, Y., Accurate and Simple Analytic Representation of the Electron-Gas Correlation-Energy. *Phys Rev B* **1992,** *45* (23), 13244-13249.
79. Perdew, J. P.; Burke, K.; Wang, Y., Generalized Gradient Approximation for the Exchange-Correlation Hole of a Many-Electron System. *Phys Rev B* **1996,** *54* (23), 16533-16539.
80. Burke, K.; Perdew, J. P.; Wang, Y., Derivation of a Generalized Gradient Approximation: The PW91 Density Functional. In *Electronic Density Functional Theory: Recent Progress and New Directions*, Dobson, J. F.; Vignale, G.; Das, M. P., Eds. Plenum: New York, 1997; pp 81-122.
81. Lee, T. J.; Taylor, P. R., A Diagnostic for Determining the Quality of Single-Reference Electron Correlation Methods. *Int J Quantum Chem* **1989**, 199-207.
82. Deegan, M. J. O.; Knowles, P. J., Perturbative Corrections to Account for Triple Excitations in Closed and Open-Shell Coupled-Cluster Theories. *Chem Phys Lett* **1994,** *227* (3), 321-326.
83. Rittby, M.; Bartlett, R. J., An Open-Shell Spin-Restricted Coupled Cluster Method - Application to Ionization-Potentials in N-2. *J Phys Chem* **1988,** *92* (11), 3033-3036.
84. Knowles, P. J.; Hampel, C.; Werner, H. J., Coupled-Cluster Theory for High-Spin, Open-Shell Reference Wave-Functions. *J Chem Phys* **1993,** *99* (7), 5219-5227.
85. Werner, H.-J.; Knowles, P. J.; Knizia, G.; Manby, F. R.; Schütz, M.; Celani, P.; Györffy, W.; Kats, T.; Korona, T.; Lindh, R., et al. *MOLPRO version 2018.1*, 2018.
86. Werner, H.-J.; Knowles, P. J.; Knizia, G.; Manby, F. R.; Schutz, M., Molpro: a General-Purpose Quantum Chemistry Program Package. *Wires Comput Mol Sci* **2012,** *2* (2), 242-253.
87. Reed, A. E.; Curtiss, L. A.; Weinhold, F., Intermolecular Interactions from a Natural Bond Orbital, Donor-Acceptor Viewpoint. *Chem Rev* **1988,** *88* (6), 899-926.
88. Glendening, E. D.; Badenhoop, J. K.; Reed, A. E.; Carpenter, J. E.; Bohmann, J. A.; Morales, C. M.; Karafiloglou, P.; Landis, C. R.; Weinhold, F. *Natural Bond Order 7.0*, Theoretical Chemistry Institute, University of Wisconsin: Madison, WI, 2018.
89. Glendening, E. D.; Landis, C. R.; Weinhold, F., NBO 7.0: New Vistas in Localized and Delocalized Chemical Bonding Theory. *J Comput Chem* **2019,** *40* (25), 2234-2241.
90. Hunter, E. P. L.; Lias, S. G., Evaluated Gas Phase Basicities and Proton Affinities of Molecules: An Update. *J Phys Chem Ref Data* **1998,** *27*, 413-656.
91. Buhl, M.; Sieffert, N.; Chaumont, A.; Wipff, G., Water versus Acetonitrile Coordination to Uranyl. Density Functional Study of Cooperative Polarization Effects in Solution. *Inorg Chem* **2011,** *50* (1), 299-308.
92. Soderholm, L.; Skanthakumar, S.; Neuefeind, J., Determination of Actinide Speciation in Solution Using High-Energy X-ray Scattering. *Anal Bioanal Chem* **2005,** *383* (1), 48-55.
93. Shannon, R. D., Revised Effective Ionic-Radii and Systematic Studies of Interatomic Distances in Halides and Chalcogenides. *Acta Crystallogr A* **1976,** *32* (Sep1), 751-767.
94. Edelstein, N. M.; Fuger, J.; Katz, J. J.; Morss, L. R., Summary and Comparison of Properties of the Actinide and Transactinide Elements. In *The Chemistry of the Actinde and Transactinde Elements*, 4 ed.; Morss, L. R.; Edelstein, N. M.; Fuger, J.; Katz, J. J., Eds. Springer: Dordrecht, Netherlands, 2006; Vol. 3, pp 1753-1835.
95. Feyel, S.; Schroder, D.; Schwarz, H., Gas-Phase Chemistry of Vanadium Oxide Cluster Cations VmOn+ (m=1-4; n=1-10) with Water and Molecular Oxygen. *Eur J Inorg Chem* **2008,** (31), 4961-4967.
96. Vasiliu, M.; Gibson, J. K.; Peterson, K. A.; Dixon, D. A., Gas Phase Hydrolysis and Oxo-Exchange of Actinide Dioxide Cations: Elucidating Intrinsic Chemistry from Protactinium to Einsteinium. *Chem-Eur J* **2019,** *25* (17), 4245-4254.
97. Bratsch, S. G.; Lagowski, J. J., Actinide Thermodynamic Predictions .3. Thermodynamics of Compounds and Aquo Ions of the 2+, 3+, and 4+ Oxidation-States and Standard Electrode-Potentials at 298.15 K. *J Phys Chem* **1986,** *90* (2), 307-312.

98. Kramida, A.; Ralchenko, Y.; Reader, J.; Team, N. A. NIST Atomic Spectra Database (ver. 5.7.1) [Online]. https://physics.nist.gov/asd (accessed June 5, 2020).
99. Afeefy, H. Y.; Liebman, J. F.; Stein, S. E.; Burgess, D. R. J. NIST Chemistry WebBook, NIST Standard Reference Database Number 69. https://webbook.nist.gov/chemistry.
100. Marçalo, J.; Gibson, J. K., Gas-Phase Energetics of Actinide Oxides: An Assessment of Neutral and Cationic Monoxides and Dioxides from Thorium to Curium. *J Phys Chem A* **2009,** *113* (45), 12599-12606.
101. Gibson, V. C., Structural and Bonding Patterns in Tetrahedral and Pseudo-Tetrahedral Transition-Metal Complexes Containing Pi-Donor Ligands. *J Chem Soc Dalton* **1994,** (11), 1607-1618.
102. Neidig, M. L.; Clark, D. L.; Martin, R. L., Covalency in f-Element Complexes. *Coordin Chem Rev* **2013,** *257* (2), 394-406.
103. Denning, R. G., Electronic Structure and Bonding in Actinyl Ions and Their Analogs. *J Phys Chem A* **2007,** *111* (20), 4125-4143.
104. Siegbahn, P. E. M., Binding in 2nd-Row Transition-Metal Dioxides, Trioxides, Tetraoxides, Peroxides, and Superoxides. *J Phys Chem* **1993,** *97* (36), 9096-9102.
105. Kaltsoyannis, N., Covalency Hinders AnO(2)(H2O)(+) -> AnO(OH)(2)(+) Isomerisation (An = Pa-Pu). *Dalton T* **2016,** *45* (7), 3158-3162.

TOC Graphic

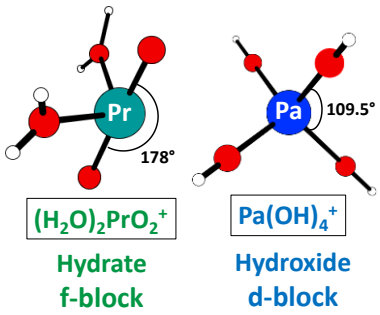
Pr
178°
Pa
109.5°
$(H_2O)_2PrO_2^+$
$Pa(OH)_4^+$
Hydrate
f-block
Hydroxide
d-block